BOEING SCIENTIFIC RESEARCH LABORATORIES DOCUMENT D1-82-0855

BOEING

SCIENTIFIC RESEARCH LABORATORIES

Compressible Boundary Layer Stability by Time Integration of the Navier-Stokes Equations and An Extension of Emmons' Transition Theory to Hypersonic Flow

A. L. Nagel

FLIGHT SCIENCES LABORATORY SEPTEMBER 1967

DISCLAIMER NOTICE

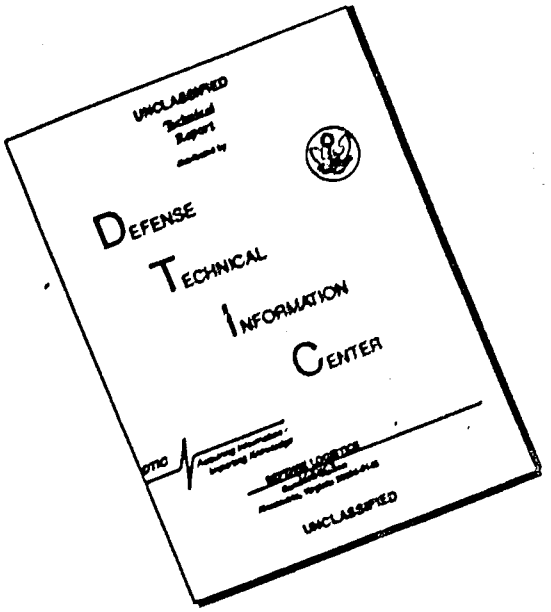

THIS DOCUMENT IS BEST QUALITY AVAILABLE. THE COPY FURNISHED TO DTIC CONTAINED A SIGNIFICANT NUMBER OF PAGES WHICH DO NOT REPRODUCE LEGIBLY.

D1-82-0655

BOEING SCIENTIFIC RESEARCH LABORATORIES

Flight Sciences Laboratory Report No. 119

COMPRESSIBLE BOUNDARY LAYER STABILITY BY TIME INTEGRATION OF THE NAVIER-STOKES EQUATIONS and AN EXTENSION OF EMMONS' TRANSITION THEORY TO HYPERSONIC FLOW

A. L. Nagel

September 1967

PREFACE

This report contains the text of a paper given at a Boundary Layer Transition Study Group meeting held at Aerospace Corporation, San Bernardino, California, July 11, 1967. The research reported here was begun in the Space Division of The Boeing Company and completed at the Boeing Scientific Research Laboratory. The author wishes to acknowledge several sources of assistance in the work described herein: to Mr. R. T. Savage of The Boeing Company, who worked with the author during the early stages of the stability work; to Dr. H. Fiedler of the Boeing Scientific Research Laboratories, for many helpful discussions related to the transition study, and for the specific suggestion that λ_z might be related to the turbulence scale; to Dr. Arnold Goldburg of the Boeing Scientific Research Laboratories, who obtained for the author an appointment to the Boeing Scientific Research Laboratories to continue work on these studies; and to the Air Force Flight Dynamics Laboratory, under whose financial support the stability study was begun.

COMPRESSIBLE BOUNDARY LAYER STABILITY BY TIME-INTEGRATION OF THE NAVIER-STOKES EQUATIONS, AND AN EXTENSION OF EMMONS' TRANSITION THEORY TO HYPERSONIC FLOW

A. L. Nagel

The Boeing Company, Seattle, Washington

INTRODUCTION AND SUMMARY

This paper presents results from two separate studies related to transition. The first part describes boundary layer stability calculations based on the direct numerical integration of the Navier-Stokes Equations with respect to time. The purpose of reformulating the stability problem in the present manner is to avoid the inherent linearization of the classical method. The study that led to the present results is viewed as the initial phase of the development of a numerical method capable of treating transition itself, although it is too early to say just how far into the transition zone the method can be extended.

The first phase of such a study consists of developing adequate numerical techniques for the integration and for representing boundary conditions. Although the complexity of the basic equations precludes rigorous numerical analysis, it is believed that this first stage of development has been completed. Numerical experiments and comparisons between the present calculations and those obtained by other methods show the numerical integration scheme reported here to be highly accurate. For example, it is shown that the amplification rates given by the present method agree with those given by the classical method over a range of Reynolds numbers encompassing both branches of the neutral curve. The resolution of the upper branch represents an especially severe test of the accuracy of the numerical scheme. In the purely numerical experiments, it is shown that the accumulated numerical error is much less than 0.1 percent after 1000 time steps and much less than 1 percent of the computed physical amplification occurring during the same period.

No survey of boundary layer stability results is given in this paper, since at the present time each calculation is restricted to a specific

combination of wavelength and Reynolds number, requiring many individual cases to be calculated in searching for the neutral curve. Rather, present efforts are directed toward the development of a more efficient method of determining critical Reynolds numbers, using the unique capabilities that the present method provides. One very simple and promising technique is described wherein the Reynolds number is varied during the calculation. It is shown that this technique can provide the entire amplification rate curve (for a constant wavelength) with a single calculation but, as might be expected, these results exhibit lag effects. The study of this lag effect continues, but it is to be noted that an analogous effect is expected to occur in actual flow experiments, due to the streamwise growth of the boundary layer.

As an example of the ease with which more complicated flows can be analyzed by the present method, a calculation has been made that includes the nonlinear Reynolds stress effect on the steady flow profile. Although the distortion is small, it is found that the distorted profile is much more unstable than was the original profile. Neither the variable Reynolds number calculations nor the addition of the Reynolds stress calculation required any appreciable increase in computer time over the simpler constant base-flow calculations.

The second part of the paper presents an application of Emmons' transition theory in hypersonic flow. Following Emmons, it is assumed that transition begins with the formation of turbulent spots that increase in size as they are swept downstream, eventually merging to form a fully turbulent boundary layer. Based on experimental results, it is assumed that the shape and velocity of the turbulent spots are independent of the Reynolds number and that their size increase linearly with distance. An expression for the local intermittency factors is then derived, and a scaling rule for transition is obtained. A key factor in the scaling of transition data is shown to be the frequency of spot formation. A dimensional argument is used to obtain an expression for the frequency of spot formation, and that expression is found to require the existence of a characteristic length that may be identified as the average spanwise spacing of the turbulent spots. Some well-known experimental and theoretical results are noted in support of the proposition that this characteristic length is not determined by the

local boundary layer flow, but for wind tunnel flow is related to the scale of freestream turbulence. In hypersonic wind tunnels, where the freestream turbulence has been shown to be prima ily due to noise radiated from turbulent boundary layers on the tunnel walls, it is predicted that the Reynolds number of transition on a flat plate model will increase as the 0.4 power of th the Reynolds number based on the tunnel diameter. Hence, a normalized Reynolds number

$$\overline{Re}_T = \frac{Re_T}{(Re_D)^{0.4}}$$

is proposed as a correlating parameter for hypersonic wind tunnel transition data. In any given wind tunnel of constant test section size, it is predicted that the transition Reynolds number on flat plate models will increase as the 0.4 power of the Reynolds number per foot. Thus, the present analysis provides a possible explanation of the so-called "unit Reynolds number effect" that has been observed in many experiments related to boundary layer transition.

The argument leading to the prediction of a tunnel diameter effect implies that there will be some effect of tunnel shape on transition, and so $\overline{Re}_T$ is not expected to correlate data from different wind tunnels unless the tunnels are geometrically similar. However, it is shown that data from two rectangular wind tunnels of different size but similar geometries are in close agreement when plotted in terms of $\overline{Re}_T$, and that approximate agreement with data from circular tunnels is also obtained.

The effect of leading edge sweep on transition was also investigated, assuming that sweep has no effect on any of the properties of turbulent spots or their rate of formation. This calculation is somewhat more speculative than those for unswept plates, since there are no published observations of the behavior of turbulent spots on swept plates. However, it is shown that the limited amount of data available is in good agreement with the theory, both as to the effect of tunnel unit Reynolds number and as to the effect of leading edge sweep. Some data that appear to show a different sweep effect are shown to be influenced by the corners of the test model. When correction is made for the corner effect, the theory is brought into approximate agreement with these data as well. The correction for the corner effect does not involve

any additional assumptions, but merely accounts for the difference between the planform of the experimental model and that of the infinite-span swept plate assumed in the theory.

A calculation of the effect of Mach number is attempted, assuming that a dimensionless frequency appearing in the theory is related the frequency of the most highly amplified Tollmien-Schlichting wave. The predicted effect is in reasonable agreement with experimental results for Mach number from 4 to 8, but falls below the data at a Mach number of 10. There is good reason to believe that certain other parameters appearing in the theory are also Mach number dependent, and experimental evidence indicates that at least one of these (the spot velocity) is varying in a manner tha would improve the agreement at Mach 10. However, in the absence of definite information, the author prefers not to speculate on these possible effects other than to note that little variation in the additional parameters would be required to yield very close agreement. Similarly, in the absence of reported observations of turbulent spots for other geometries, the author has not attempted to calculate transition trends for shapes other than sharp flat plates (with and without leading edge sweep) and flow-aligned hollow cylinders. There is no conceptual difficulty in making such calculations, however, and there is experimental evidence that the trends computed for flat plates also occur on other geometries and in hypersonic wakes.

Some discussion of the implications of the present transition theory regarding the relation of wind tunnel data to those of actual flight is also given. It appears that either flight transition Reynolds numbers will be much higher than those obtained in wind tunnels or that a unit Reynolds number effect will also be observed in flight. In the latter event, it is predicted that the in-flight unit Reynolds number effect will be a square-root relationship.

PART I

CALCULATION OF THE STABILITY OF THE COMPRESSIBLE LAMINAR BOUNDARY LAYER BY TIME INTEGRATION OF THE NAVIER-STOKES EQUATIONS

The physical situation being analyzed here is the stability of a laminar boundary layer over a flat plate. The oncoming flow is uniform far upstream of the plate. The leading edge of the plate is normal to the flow, and the plate is of infinite span, so that the flow over the plate is two-dimensional. There is a thin layer of fluid (the boundary layer) near the plate wherein the velocity of the fluid decreases from its uniform value to zero at the plate surface. The flow in the boundary layer is basically steady and assumed known from boundary layer theory. The flow is compressible and its transport properties are functions of the temperature. The analysis is concerned with the behavior of infinitesimal disturbances to the steady flow. In the present study, the disturbances are considered known at some initial time so that the analysis becomes an initial value problem.

Mathematical Formulation

The equations for the conservation of mass, momentum and energy for a two-dimensional compressible fluid may be written as:*

$$\begin{aligned} \frac{\partial u}{\partial t} &= \dot{u}(u, v, e, H) \\ \frac{\partial v}{\partial t} &= \dot{v}(u, v, e, H) \\ \frac{\partial e}{\partial t} &= \dot{e}(u, v, e, H) \\ \frac{\partial H}{\partial t} &= \dot{H}(u, v, e, H) \end{aligned} \qquad (1)$$

Also required are the equation of state,

$$P = \rho R T$$

---

*Symbols are defined in the Appendix.

and auxiliary equations for the fluid properties, e.g.,

$$\mu = \mu(T)$$

For the present purpose, it is useful to decompose the flow into a steady laminar flow and unsteady perturbations. Such decomposition does not necessarily involve any approximation since every flow could be written in this manner. In particular, such decomposition does not necessarily imply linearization. The motivation for the decomposition in the present study is increased accuracy and easier interpretation of results; the equations themselves are much more complicated than the original conservation equations. The decomposition also allows the use of approximate laminar flow solutions without introducing any time-dependent errors into the calculations. This is done by deleting all terms that involve only steady flow quantities, including their time derivatives, and is equivalent to assuming that the prescribed laminar steady flow satisfies the conservation equations exactly. The resulting equations are reproduced in Table I.

Numerical Formulation

For numerical computation it is necessary to replace the differential equations of Table I by finite difference analogs. The first step in formulating the finite difference analogs is to replace the spatial derivatives by numerical forms. In the present method, the flow field is represented by an x-y plane, with x and y divided into uniform increments $\triangle x$ and $\triangle y$. All calculations are carried out at the mesh points for which

$$x = m \cdot \triangle x$$
$$y = n \cdot \triangle y$$

with m and n being integers. The increments, $\triangle x$ and $\triangle y$, are uniform but not necessarily equal. Having set up the mesh array, three steps are required for the numerical formulation: replacing spatial derivatives by finite difference expressions, replacing time integration by a suitable

Table 1: CONSERVATION EQUATIONS

Mass Conservation:

$$\frac{\partial \rho'}{\partial t} = -\left[\frac{\partial}{\partial x}\left(\rho'\bar{u} + \bar{\rho}u' + \rho'u'\right) + \frac{\partial}{\partial y}\left(\rho'\bar{v} + \bar{\rho}v' + \rho'v'\right)\right] \qquad \text{(I)}$$

x-Momentum:

$$\begin{aligned}\frac{\partial \bar{u}'}{\partial t} = &-\left[\bar{u}\frac{\partial u'}{\partial x} + u'\frac{\partial \bar{u}}{\partial x} + u'\frac{\partial u'}{\partial x} + \bar{v}\frac{\partial u'}{\partial y}\right. \\ &\left. + v'\frac{\partial \bar{u}}{\partial y} + v'\frac{\partial u'}{\partial y} + \frac{\rho'}{\bar{\rho}+\rho'}\left(\bar{u}\frac{\partial \bar{u}}{\partial x} + \bar{v}\frac{\partial \bar{u}}{\partial y}\right)\right] \\ &+ \frac{1}{\bar{\rho}+\rho'}\left\{-\frac{\partial P'}{\partial x} + \frac{\partial}{\partial x}\left[\mu'\left(\frac{4}{3}\frac{\partial \bar{u}}{\partial x} + \frac{1}{3}\frac{\partial u'}{\partial x} - \frac{2}{3}\frac{\partial \bar{v}}{\partial y} - \frac{2}{3}\frac{\partial v'}{\partial y}\right)\right.\right. \\ &\left. + \bar{\mu}\left(\frac{4}{3}\frac{\partial u'}{\partial x} - \frac{2}{3}\frac{\partial v'}{\partial y}\right)\right] + \frac{\partial}{\partial y}\left[\mu'\left(\frac{\partial \bar{u}}{\partial y} + \frac{\partial u'}{\partial y} + \frac{\partial \bar{v}}{\partial x} + \frac{\partial v'}{\partial x}\right)\right. \\ &\left.\left. + \bar{\mu}\left(\frac{\partial u'}{\partial y} + \frac{\partial v'}{\partial x}\right)\right]\right\}\end{aligned} \qquad \text{(II)}$$

y-Momentum:

$$\begin{aligned}\frac{\partial \bar{v}'}{\partial t} = &-\left[\bar{v}\frac{\partial v'}{\partial y} + v'\frac{\partial \bar{v}}{\partial y} + v'\frac{\partial v'}{\partial y} + \bar{u}\frac{\partial v'}{\partial x}\right. \\ &\left. + u'\frac{\partial \bar{v}}{\partial x} + u'\frac{\partial v'}{\partial x} + \frac{\rho'}{\bar{\rho}+\rho'}\left(\bar{v}\frac{\partial \bar{v}}{\partial y} + \bar{u}\frac{\partial \bar{v}}{\partial x}\right)\right] \\ &+ \frac{1}{\bar{\rho}+\rho'}\left\{-\frac{\partial P'}{\partial y} + \frac{\partial}{\partial x}\left[\mu'\left(\frac{4}{3}\frac{\partial \bar{v}}{\partial y} + \frac{1}{3}\frac{\partial v'}{\partial y} - \frac{2}{3}\frac{\partial \bar{u}}{\partial x} - \frac{2}{3}\frac{\partial u'}{\partial x}\right)\right.\right. \\ &\left. + \bar{\mu}\left(\frac{4}{3}\frac{\partial v'}{\partial y} - \frac{2}{3}\frac{\partial u'}{\partial x}\right)\right] + \frac{\partial}{\partial x}\left[\mu'\left(\frac{\partial \bar{v}}{\partial x} + \frac{\partial v'}{\partial x} + \frac{\partial \bar{u}}{\partial y} + \frac{\partial u'}{\partial y}\right)\right. \\ &\left.\left. + \bar{\mu}\left(\frac{\partial v'}{\partial x} + \frac{\partial u'}{\partial y}\right)\right]\right\}\end{aligned} \qquad \text{(III)}$$

Energy:

$$\begin{aligned}\frac{\partial \bar{H}'}{\partial t} = &-\left[\bar{u}\frac{\partial H'}{\partial x} + u'\frac{\partial \bar{H}}{\partial x} + u'\frac{\partial H'}{\partial x} + \bar{v}\frac{\partial H'}{\partial y}\right. \\ &\left. + v'\frac{\partial \bar{H}}{\partial y} + v'\frac{\partial H'}{\partial y} + \frac{\rho'}{\bar{\rho}+\rho'}\left(\bar{u}\frac{\partial \bar{H}}{\partial x} + \bar{v}\frac{\partial \bar{H}}{\partial y}\right)\right]\end{aligned} \qquad \text{(IV)}$$

Table I (Continued)

$$+ \frac{1}{\bar{\rho} + \rho'} - \left\{ \frac{\partial P'}{\partial t} + \frac{\partial}{\partial x} \left[\frac{\bar{\mu}}{Pr} \frac{\partial H'}{\partial x} + \frac{\mu'}{Pr} \frac{\partial \bar{H}}{\partial x} + \frac{\mu'}{Pr} \frac{\partial H'}{\partial x} \right.\right.$$

$$+ (\bar{\mu} + \mu') \left(1 - \frac{1}{Pr}\right) \left(\bar{v} \frac{\partial v'}{\partial x} + v' \frac{\partial \bar{v}}{\partial x} + v' \frac{\partial v'}{\partial x} \right)$$

$$+ \mu' \left(1 - \frac{1}{Pr}\right) \bar{v} \frac{\partial \bar{v}}{\partial x} + (\bar{\mu} + \mu') \left(\frac{4}{3} - \frac{1}{Pr}\right) \left(\bar{u} \frac{\partial u'}{\partial x} \right.$$

$$\left.\left. + u' \frac{\partial \bar{u}}{\partial x} + u' \frac{\partial u'}{\partial x} \right) + \mu' \left(\frac{4}{3} - \frac{1}{Pr}\right) \left(\bar{u} \frac{\partial \bar{u}}{\partial x} \right) \right]$$

$$+ \frac{\partial}{\partial y} \left[\frac{\bar{\mu}}{Pr} \frac{\partial H'}{\partial y} + \frac{\mu'}{Pr} \frac{\partial \bar{H}}{\partial y} + \frac{\mu'}{Pr} \frac{\partial H'}{\partial y} \right.$$

$$+ (\bar{\mu} + \mu') \left(1 - \frac{1}{Pr}\right) \left(\bar{u} \frac{\partial u'}{\partial y} + u' \frac{\partial \bar{u}}{\partial y} + u' \frac{\partial u'}{\partial y} \right)$$

$$+ \mu' \left(1 - \frac{1}{Pr}\right) \bar{u} \frac{\partial \bar{u}}{\partial y} + (\bar{\mu} + \mu') \left(\frac{4}{3} - \frac{1}{Pr}\right) \left(\bar{v} \frac{\partial v'}{\partial y} \right.$$

$$\left.\left. + v' \frac{\partial \bar{v}}{\partial y} + v' \frac{\partial v'}{\partial y} \right) + \mu' \left(\frac{4}{3} - \frac{1}{Pr}\right) \left(\bar{v} \frac{\partial \bar{v}}{\partial y} \right) \right]$$

$$+ (\bar{\mu} + \mu') \left[\frac{1}{3} \left(\bar{u} \frac{\partial^2 v'}{\partial x \partial y} + u' \frac{\partial^2 \bar{v}}{\partial x \partial y} + u' \frac{\partial^2 v'}{\partial x \partial y} \right.\right.$$

$$\left. + \bar{v} \frac{\partial^2 u'}{\partial x \partial y} + v' \frac{\partial^2 \bar{u}}{\partial x \partial y} + v' \frac{\partial^2 u'}{\partial x \partial y} \right)$$

$$+ 2 \left(\frac{\partial \bar{v}}{\partial x} \frac{\partial u'}{\partial y} + \frac{\partial v'}{\partial x} \frac{\partial \bar{u}}{\partial y} + \frac{\partial v'}{\partial x} \frac{\partial u'}{\partial y} \right)$$

$$\left. - \frac{4}{3} \left(\frac{\partial \bar{u}}{\partial x} \frac{\partial v'}{\partial y} + \frac{\partial u'}{\partial x} \frac{\partial \bar{v}}{\partial y} + \frac{\partial u'}{\partial x} \frac{\partial v'}{\partial y} \right) \right]$$

$$+ \mu' \left[\frac{1}{3} \left(\bar{u} \frac{\partial^2 \bar{v}}{\partial x \partial y} + \bar{v} \frac{\partial^2 \bar{u}}{\partial x \partial y} \right) + 2 \frac{\partial \bar{v}}{\partial x} \frac{\partial \bar{u}}{\partial y} \right.$$

$$\left. - \frac{4}{3} \frac{\partial \bar{u}}{\partial x} \frac{\partial \bar{v}}{\partial y} \right] + \frac{\partial}{\partial x} (\bar{\mu} + \mu') \left[- \frac{2}{3} \left(\bar{u} \frac{\partial v'}{\partial y} \right.\right.$$

$$\left.\left. + u' \frac{\partial \bar{v}}{\partial y} + u' \frac{\partial v'}{\partial y} \right) + \bar{v} \frac{\partial u'}{\partial y} + v' \frac{\partial \bar{u}}{\partial y} + v' \frac{\partial u'}{\partial y} \right]$$

Table I (Concluded)

$$+ \frac{\partial \mu'}{\partial x}\left(-\frac{2}{3}\bar{u}\frac{\partial \bar{v}}{\partial y} + \bar{v}\frac{\partial \bar{u}}{\partial y}\right) + \frac{\partial}{\partial y}(\bar{\mu} + \mu')\left[-\frac{2}{3}\left(\bar{v}\frac{\partial u'}{\partial x} + v'\frac{\partial \bar{u}}{\partial x} + v'\frac{\partial u'}{\partial x}\right) + \bar{u}\frac{\partial v'}{\partial x} + u'\frac{\partial \bar{v}}{\partial x} + u'\frac{\partial v'}{\partial x}\right]$$

$$+ \frac{\partial \mu'}{\partial y}\left(-\frac{2}{3}\bar{v}\frac{\partial \bar{u}}{\partial x} + \bar{u}\frac{\partial \bar{v}}{\partial x}\right)\Bigg\}$$

Equation of State:

$$P' = R(\bar{\rho}\,T' + \rho'\,\bar{T} + \rho'\,T') \qquad (V)$$

Viscosity Law:

$$\mu' = (0.2325 \times 10^{-8})\left[\frac{(\bar{T} + T')^{3/2}}{\bar{T} + T' + 216} - \frac{\bar{T}^{3/2}}{\bar{T} + 216}\right] \qquad (VI)$$

Enthalpy-Temperature Relationships:

$$H' = c_p\,T' + \bar{u}\,u' + \frac{u'^2 + v'^2}{2} \qquad (VII)$$

numerical scheme and devising satisfactory numerical representations of the boundary conditions.

1. Spatial Derivatives

Since the flow properties are known only at discrete points, it is necessary to approximate the flow field properties by functions that can be differentiated to obtain the required spatial derivatives. There exist infinitely many approximating functions that could be used that would all yield exact results in the limit as $\triangle x$ and $\triangle y$ approach zero. Since $\triangle x$ and $\triangle y$ must remain finite in any actual calculation, it is necessary to find that method that yields the best results for finite spatial increments.

The most obvious and most commonly used approximating functions are polynomials, and polynomials were used in all of the present studies. A polynomial of degree n is uniquely determined by n + 1 conditions, which may be conditions on either the values or the derivatives of the polynomials. In numerical flow studies, the commonly applied conditions are that the polynomials agree with the values of the flow field properties at the surrounding mesh points. After some study, it was decided that polynomial curve fits should be used, and since no derivative higher than the second is required, three-point central difference formulae were used. It would appear that higher order polynomials should theoretically yield more accurate results, but the computations have not borne this out.

Uncentered difference formulae were also investigated in some cases in attempts to suppress spurious mesh-frequency oscillations. It was found that the uncentered differences suppress such oscillations, but also cause systematic trends to appear. The direction of the trends were reversed when the direction of uncentering was reversed, proving that the trends were purely numerical effects. The use of uncentered differences was therefore discontinued. The spurious oscillations were later found to originate at the boundaries and disappeared when the boundary condition equations described herein were used.

2. Time Integration Scheme

As with spatial derivatives, there will also exist infinitely many numerical analogs for a given differential equation that are equivalent in the sense that all will approach the differential equation in the limit as the step size is decreased to zero. For finite step sizes, however, these schemes may have different properties, and again it is necessary to search for the method that yields the best results for a given amount of computer time. The requirements of the numerical scheme for the present study are unusually severe, since the physical problem under consideration involves a delicate balance between relatively large but opposing physical effects, and further, that balance may itself be unstable.

Broadly speaking, numerical schemes are subject to two types of inaccuracy. The first form, numerical instability, may occur when the increment in the independent variable (time, in the present study) exceeds some critical value. If the increments exceed this critical value, the numerical results oscillate erratically, usually with ever-growing amplitudes, and do not even approximate a true solution of the differential equation. If the step size is held sufficiently small to avoid numerical instability, it is still found that the computed results vary somewhat with step size. This effect is due to truncation error; that is, to the failure of the numerical scheme to include all of the terms in the Taylor Series (about the time t) in stepping forward to the time $t + \Delta t$. The truncation error can be reduced by increasing the order of the integration scheme or by further reducing the step size. Of course, the step size cannot be reduced indefinitely without making the number of calculations excessive.

A rigorous analysis of the stability and convergence characteristics of the numerical analogs to the equations of Table I is precluded by the complexity of those equations. However, as discussed more fully in Reference 1, two fruitful avenues are open: 1) a thorough analysis of similar but simpler equations, and 2) numerical experiments with the complete equations. Thus, the individual engaged in a numerical study of the present type is in much the same situation as an experimentalist, having the ability to vary experimental parameters and having approximate theories for guidance, but lacking in absolute proof that his results are correct.

Perhaps the most obvious numerical integration scheme is first order forward integration, which may be written as:

$$\text{Steps 1 - 4:} \quad \text{Calculate} \quad \frac{dQ_i}{dt} \tag{2a}$$

$$\text{Steps 5 - 8:} \quad Q_i(t+\Delta t) = Q_i(t) + \Delta t \frac{\partial Q_i}{\partial t} \tag{2b}$$

where the Q_i stand for u, v, ρ, and H. However, the truncation error of this system is unacceptably large. As described in Reference 1, a much better scheme is obtained by merely altering the sequence of calculation as follows:

1) Compute $\frac{\partial \rho}{\partial t}$ and $\frac{\partial H}{\partial t}$ (Eqn. 2a)
2) Update ρ and H (Eqn. 2b)
3) Compute $\frac{\partial u}{\partial t}$ and $\frac{\partial v}{\partial t}$ (Eqn. 2a)
4) Update u and v (Eqn. 2b)

By assigning integral time levels n to ρ and H, and time levels $n + \frac{1}{2}$ to u and b, it was shown in Reference 1 that the resequenced scheme is a time-centered scheme but with some inconsistency in time levels. In the present scheme, which is given in Table II, this inconsistency is approximately corrected, although, as stated in Reference 1, its effect appears to be very small. The approximate correction uses a previously-computed time derivative to remove the unleveling, and so requires only one additional multiply-and-add operation for each of the four dependent variables, with only a small increase in computing time.

With the aid of simplified equations, four separate numerical stability criteria were identified, and subsequently, verified with computer experiments with the complete equations. They are:

1) $\Delta t < \frac{1.5\ \Delta x}{\sqrt{\gamma RT}}$

2) $\Delta t < \frac{\Delta x}{\sqrt{2\ u_e}}$

} obtained from the continuity equation and the inviscid part of the momentum equations

TABLE II: NUMERICAL INTEGRATION SCHEME

Stored from Previous Calculation: ρ^n, H^n, $\dot{\rho}^{n-\frac{1}{2}}$, $\dot{H}^{n-\frac{1}{2}}$, $u^{n+\frac{1}{2}}$, $v^{n+\frac{1}{2}}$, $\dot{u}^n$, $\dot{v}^n$

Note: $\rho^n \equiv \rho(n\Delta t)$. $\dot{\rho} \equiv \frac{\partial \rho}{\partial t}$

Step 1. $\rho^{n+\frac{1}{2}} = \rho^n + \frac{1}{2}\Delta t\, \dot{\rho}^{n-\frac{1}{2}}$

Step 2. $H^{n+\frac{1}{2}} = H^n + \frac{1}{2}\Delta t\, \dot{H}^{n-\frac{1}{2}}$

Step 3. $\dot{\rho}^{n+\frac{1}{2}} = \dot{\rho}\left(\rho^{n+\frac{1}{2}}, H^{n+\frac{1}{2}}, u^{n+\frac{1}{2}}, v^{n+\frac{1}{2}}\right)$

Step 4. $\dot{H}^{n+} = \dot{H}\left(\rho^{n+\frac{1}{2}}, H^{n+\frac{1}{2}}, u^{n+\frac{1}{2}}, v^{n+\frac{1}{2}}\right)$

Step 5. $\rho^{n+1} = \rho^n + \Delta t\, \dot{\rho}^{n+\frac{1}{2}}$

Step 6. $H^{n+1} = H^n + \Delta t\, \dot{H}^{n+\frac{1}{2}}$

Step 7. $u^{n+1} = u^{n+\frac{1}{2}} + \frac{1}{2}\Delta t\, \dot{u}^n$

Step 8. $v^{n+1} = v^{n+\frac{1}{2}} + \frac{1}{2}\Delta t\, \dot{v}^n$

Step 9. $\dot{u}^{n+1} = \dot{u}\left(\rho^{n+1}, H^{n+1}, u^{n+1}, v^{n+1}\right)$

Step 10. $\dot{v}^{n+1} = \dot{v}\left(\rho^{n+1}, H^{n+1}, u^{n+1}, v^{n+1}\right)$

Step 11. $u^{n+3/2} = u^{n+\frac{1}{2}} + \Delta t\, \dot{u}^n$

Step 12. $v^{n+3/2} = v^{n+\frac{1}{2}} + \Delta t\, \dot{v}^n$

3) $\Delta t < \frac{\overline{\Delta x}^2}{2\nu}$ from the viscous part of the momentum equations

4) $\Delta t < \frac{\gamma \Delta x}{(\gamma-1)\overline{u}_e}$ from the energy and continuity equations

These limits were verified by comparing time histories computed for differing flow conditions with various values of Δt.

With conditions for numerical stability determined, the question of accuracy can be considered. As already noted, the accuracy of the numerical integration scheme can be assessed by varying the time step Δt and by comparison with results of other methods. Comparisons with other methods will be given in the discussion of results. Comparisons are given in Table III that show the effect of halving Δt, which, for the present integration scheme, should reduce the accumulated error by approximately three-fourths. So large a change in Δt is a rather severe test of the numerical scheme, but it is seen that after 1000 time steps this maximum difference is only .001, and is generally much smaller. Since the physical boundary layer amplification is approximately 16% in the corresponding time period, the numerical integration scheme appears to be sufficiently accurate.

Results for the same conditions computed with the earlier integration scheme are also presented in Table III. It is seen that while the differences are some four times larger than with the present method, the error is also much less than the physical amplification.

3. Boundary Conditions

Specification of boundary conditions is a crucial and difficult part of a numerical solution such as that described here, and a great deal of experimentation was required to obtain satisfactory forms. Difficulties often arise because the true boundary conditions are known only at points outside of the computed array, as is the boundary condition at y-infinity in the present case. If the boundary conditions are expressed by derivatives, there will be many possible approximations which may be equivalent only in the limiting case of zero mesh size.

TABLE III: COMPARISONS OF INTEGRATION ERRORS

j^*	$\hat{u}_j$ for $\tau = 500$			Integration Error	
	Present Scheme		Scheme of Reference 1	Effect of $\Delta\tau$	Effect of Scheme
	$\Delta\tau = .5$	$\Delta\tau = 1.0$	$\Delta\tau = .5$		
1	1.109	1.109	1.112	--	.003
2	1.162	1.162	1.166	--	.004
3	1.106	1.107	1.110	.001	.004
4	1.079	1.079	1.082	--	.003
5	1.076	1.077	1.080	.001	.004
10	.6382	.6381	.6404	.0001	.0022
16	.01171	.01191	.01169	.0002	.0002
20	.2432	.2431	.2440	.0001	.0008
30	.3181	.3178	.3191	.0003	.0010
40	.2359	.2358	.2364	.0001	.0005
60	.1259	.1259	.1265	--	.0006
80	.07014	.07049	.07088	.0003	.0007
100	.04499	.04539	.04569	.0004	.0007
120	.03600	.03620	.03700	.0002	.0010

* $y = j\,(\Delta y)$

One symptom of incorrectly formulated boundary conditions is the appearance of oscillations of wavelength $2 \cdot \Delta y$. The oscillations increase in amplitude with time, and ultimately dominate the calculations. Similar oscillations occur in much simpler systems of equations than those used here, and it has been shown that in some cases they can be suppressed by using uncentered differences for spatial derivatives. That approach was not satisfactory, as already noted. Neither are any of the 'artificial viscosity' techniques that have been so successful in inviscid flow calculations, since the present study is entirely concerned with the effects of small amounts of viscosity. An apparently satisfactory smoothing technique was used in Reference 1, but it has since been found that with the conditions described below no smoothing is required.

Wall Conditions: At the wall velocity fluctuations obey the usual boundary conditions from boundary layer theory and u' and v' are both zero. The temperature fluctuation is determined by the condition $\overline{T} + T' = T_w$. Thus, if the wall temperature does not respond to the temperature fluctuations, T' will be zero at the plate surface. The temperature response of the plate surface depends on the thermal diffusivity of the plate material. It has been assumed in the present calculations that the plate does not respond, and since u' and v' are both zero, H' is also zero at the plate surface. With the present method, it would be easily possible to allow for finite thermal capacity of the plate, but no such calculations have been made.

The wall boundary condition on density is obtained by a condition on pressure*

$$\left(\frac{\partial P'}{\partial y}\right)_w \doteq 0 \qquad (4)$$

The density perturbation is then calculated by

$$\rho'_w = P'_w \left(\frac{\overline{\rho}}{\overline{P}}\right)_w \qquad (5)$$

---

* $\left(\frac{\partial P'}{\partial y}\right)_w$ is not exactly zero because of viscous terms.

The pressure condition is approximated in the present study by a parabolic form:

$$P_w = \frac{4P_1 - 3P_2}{3} \tag{6}$$

The three conditions on the parabola are in agreement with the computed pressures at the two layers nearest the wall and the pressure derivative condition given above. Several other possibilities were investigated in the course of the present study, including time integration of the density, using the other boundary conditions.

Condition at y-Infinity: The boundary condition at y-infinity must be replaced by a condition applicable at some finite value of y. This is done by using an approximate analytic solution for the region outside of the boundary layer, namely,

$$Q_i' \sim e^{-\alpha y} \tag{7}$$

With this expression, values of u' and H' are calculated for an additional layer y_{N+1} ($y = y_{max} + \Delta y$):

$$u'_{N+1} = u'_N e^{-\alpha \Delta y}$$

and

$$H'_{N+1} = H'_N e^{-\alpha \Delta y} \tag{8}$$

It was found that the outer boundary caused less difficulty if v'_{N+1} is computed with a restricted form of the continuity equation:

$$\begin{aligned} v'_{N+1} &= v'_N + \Delta y \frac{\partial v}{\partial y} \\ &= v'_N - \Delta y \frac{\partial u}{\partial x} \end{aligned} \tag{9}$$

Condition (9) assures that $\frac{\partial p'}{\partial t}$ at the N^{th} layer will be small.

It was also found that if formulas like (8) are used to calculate P_{N+1}, oscillations can be caused. A parabolic extrapolation that agrees with (7) at y_{N+1} is

$$P_{N+1} = \frac{4P_N - 3P_{N-1}}{3 + 2\alpha\Delta y} \qquad (10)$$

Condition (10) is much less abrupt than (8) and has effectively suppressed spurious oscillations from all the cases that have been calculated.

The approximate solution (7) is valid only for incompressible flow, but the relative consistency of the various terms (i.e., (8), (9) and (10)) appears to be more important than the rate of decay assumed. Hence, condition (7) has been used for all calculations shown in this report.

Among the outer boundary condition schemes investigated was the use of backward differences. Because the coefficients appearing in uncentered difference formulae are larger than those for central differences, a more severe restriction on Δt is imposed. Failure to observe this restriction does not cause instability of the entire array, but does lead to erroneous values at the boundaries that gradually spread inward. With smaller time-steps the numerical effects are diminished, but no good scheme was found based on backward differences.

x-Boundary Conditions: The x-derivative boundary conditions are not required in the present study. Rather, it is assumed, as in classical stability theory, that all perturbations are in the form of traveling waves of a single wave number, α . Thus, we may write, for example

$$u'(x,y,t) = \hat{u}(y,t) \sin[\alpha(x-x_0)] \qquad (11)$$

With the use of Eqn. (11) the need for further specification of boundary conditions in the x direction is eliminated. The x derivatives can be specified simply and exactly as follows:

$$\frac{\partial u'}{\partial x}(x, y, t) = \alpha u'\left(x_1 + \frac{\lambda}{4}, y, t\right)$$

$$\frac{\partial u'}{\partial x}\left(x_1 + \frac{\lambda}{4}, y, t\right) = -\alpha u'(x_1, y, t) \qquad (12)$$

$$\frac{\partial^2 u}{\partial x^2}(x_1, y, t) = -\alpha^2 u'(x_1, y, t)$$

etc.

Thus, it is necessary to compute the perturbation quantities at only two x locations separated by a quarter-wavelength, and the amount of work involved in any particular computation is greatly reduced.

Results of Stability Calculations

No survey of boundary layer stability has as yet been made in the present study. The method is still under development; specifically, means are being sought for avoiding the tedious searching technique that is usually required to locate the neutral curve. An example of a promising candidate for a more direct method will be shown. Some cases that have been calculated are presented, however, primarily as indications of the type of results that can be obtained by the present method. In order to allow direct comparison with results obtained by the classical method, all terms containing products of perturbations have been deleted from the equations of Table I. The basic flow is assumed to be parallel and independent of x. The increments Δy are 0.116 δ^* and y_{max} is 14 δ^* .

Since the present stability method is in the form of an initial value problem, it is possible to trace the development of an arbitrary initial disturbance into the characteristic forms (eigen functions) given by the classical method. Two examples of such development at a Mach number of 0.4 are shown in Figure 1. In that figure, the amplitude of the u' perturbation is plotted as a function of distance above the surface for several early times. Initially, the boundary layer is disturbed by a u' pulse which is introduced at different heights in the boundary layer for the two cases shown. It is seen that the distribution soon spreads through the boundary layer, changing in distribution as time progresses. Each of the plots has been normalized so that u'_{max} is unity, and, thus, the figure does not present a true picture of the variation of disturbance amplitude with time. The amplitude is, in fact, decreasing rapidly during this formative period, since

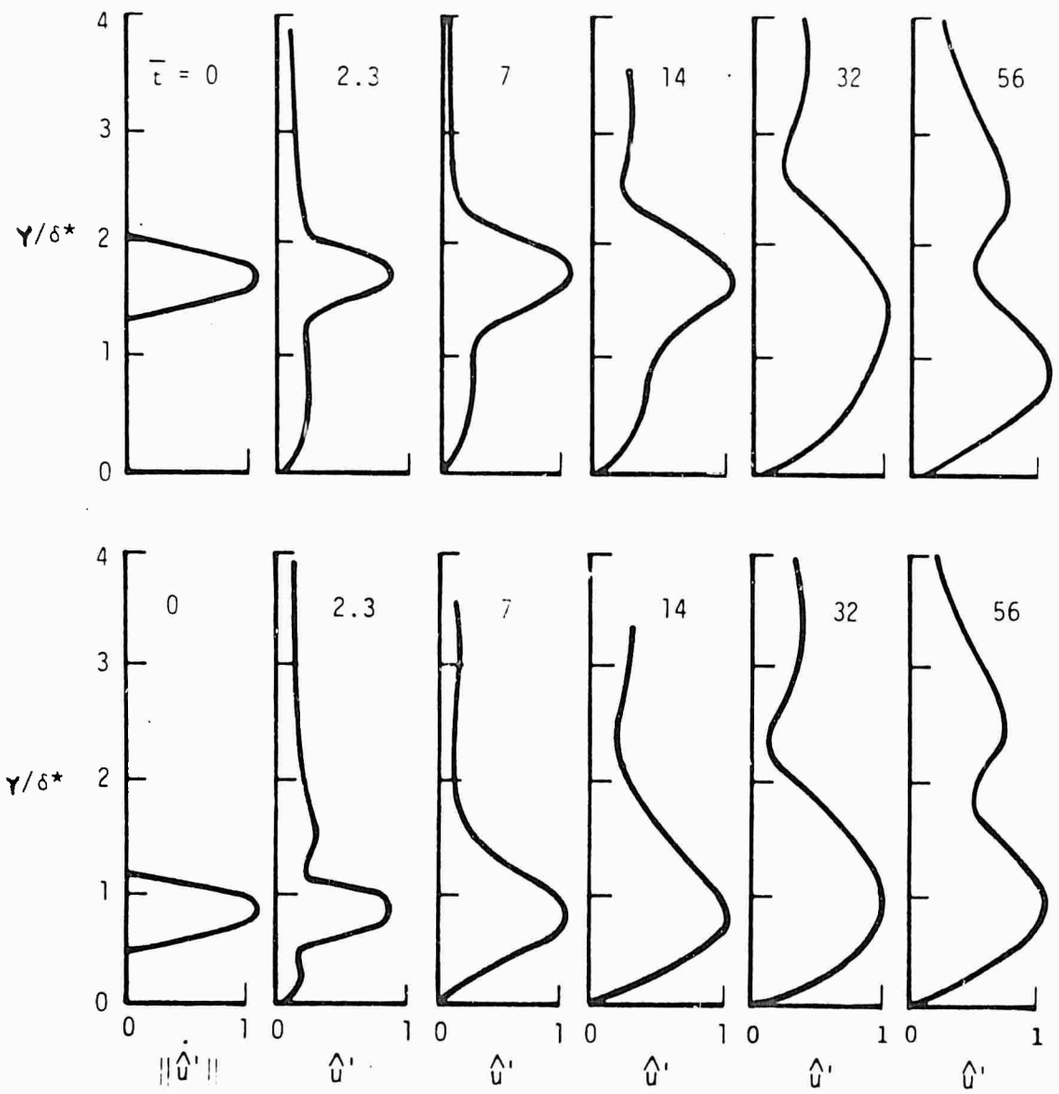

Figure 1. DEVELOPMENT OF DISTURBANCE PROFILES

M_e = 0.4, N_{Re,δ^*} = 4000

even in an unstable boundary layer, it is only certain characteristic disturbances forms that are amplified. It will be seen that at the time of the last plots shown, the distribution of disturbances within the boundary layer had become very similar in the two cases shown, although the initial disturbances were different. This is, of course, exactly the type of behavior that is anticipated on the basis of stability theory, but would be, nevertheless, very difficult to calculate by the classical (normal mode) analysis.

The final plots of Figure 1 do not represent the final disturbance profiles, however, although from that time onward the results of the two calculations are virtually indistinguishable. An example of a final profile as obtained by the present method is shown in Figure 2. It should be noted that it is only the normalized disturbance profiles that have become "final." The amplitudes of the disturbances are exponentially increasing for the case shown, since this calculation is for an unstable combination of wavelength and Reynolds number. However, when normalized by the maximum value of u', the distribution of disturbance velocities through the boundary layer is unchanging, except at the outer edge of the boundary layer. There a slight oscillation persists for a very long time, and apparently represents the reflection and re-reflection of sound waves between the surface of the plate and the outer boundary of the computed flow field, which, as previously noted, cannot be allowed to extend to infinity.

Also shown in Figure 2, for purposes of comparison, is a disturbance profile calculated by the classical method, and taken from a paper by Kurtz and Crandall (Reference 2). Exact agreement is not expected since the Kurtz and Crandall calculation is for compressible flow, while the present result is for a Mach number of 0.4. However, the differences are expected to be slight for small Mach numbers, and it is seen that the two profiles agree closely except for a small difference in the vicinity of the boundary layer outer edge.

The amplification rates obtained by the present method are compared with those of Kurtz and Crandall in Figure 3. The two sets of computed amplification rates are seen to be in approximate agreement, with the present results being slightly lower. This difference appears to be consistent with the effects of compressibility as given in previous studies. The resolution of the upper branch of the stability curve represents an especially severe

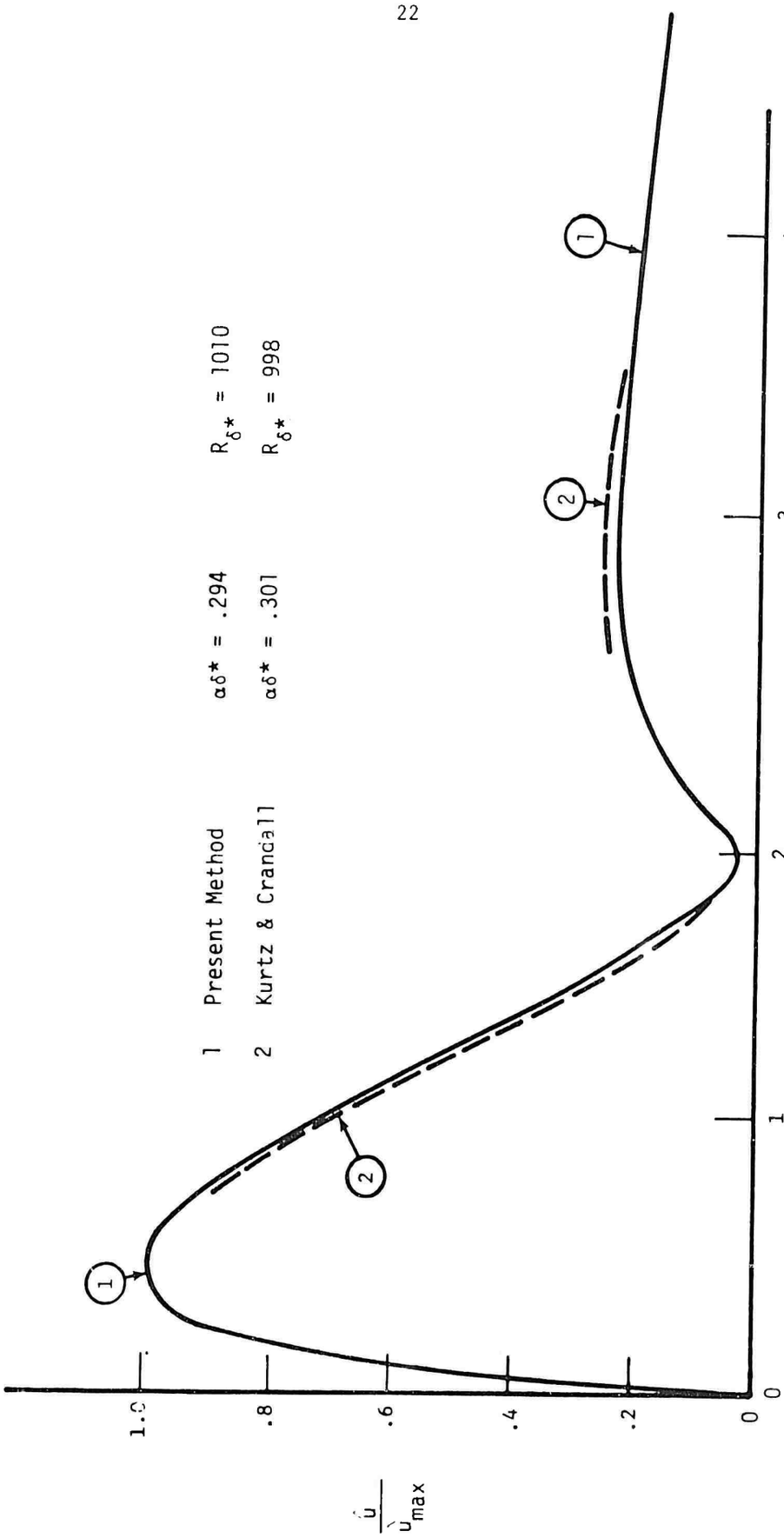

Figure 2. DISTURBANCE PROFILES AT M = 0.4

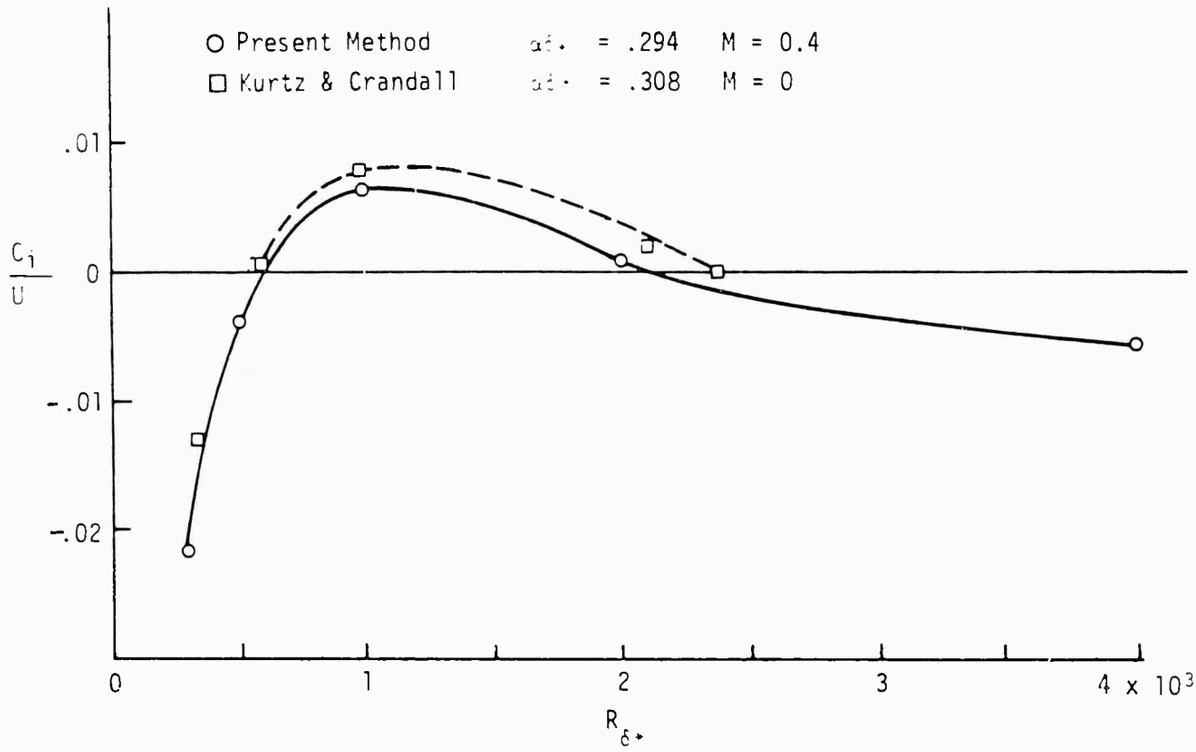

Figure 3. AMPLIFICATION RATE AT M = 0.4

test of the numerical integration scheme and boundary conditions. This upper branch could not be obtained at the time Reference 1 was published. It is now known that this failure was due indirectly to the effects of the outer boundary condition assumed there, and the smoothing technique that was used to suppress the resulting oscillations.

Figure 4 presents a calculation for a Mach number of 10. Only one case has been computed at present, which, as noted, is for a Reynolds number of 4000. This case appears to be about neutrally stable, but a critical Reynolds number cannot be determined until several more calculations have been made. Some Mach 10 calculations were also shown in Reference 1; it is now known that those cases had not yet converged, a possibility that was suggested in that report.

The present effort in the development of the method is aimed at developing a means of locating the neutral curve that avoids the necessity of performing discrete calculations at every point in the α-Re plane. One promising technique consists of allowing the Reynolds number to vary as a function of time by varying the density. An example of such a computation is shown in Figure 5. The Reynolds number at the beginning of the calculations was 100, which is well below the critical value. The Reynolds number was then increased linearly with time until the end of the calculation. The history of the u' perturbation amplitude exhibits a short-period oscillation superposed on a long term wavelike behavior. The short period oscillation is characteristic of calculations that have not yet stabilized; the long terms behavior appears to be the expected effect of the Reynolds number variation. Initially, while the Reynolds number is less than the critical value, it is expected that the disturbance amplitude should decrease. As the Reynolds number increases into the unstable range the disturbance amplitude begins to increase. When the Reynolds number is still further increased, the calculation crosses the upper branch of the neutral curve and the amplitude again begins to decrease.

The slope of the amplitude curve indicates the amplification rate. Due to the short period oscillations the original amplitude curve will not give meaningful results, but by fairing a smooth curve through the calculated values,

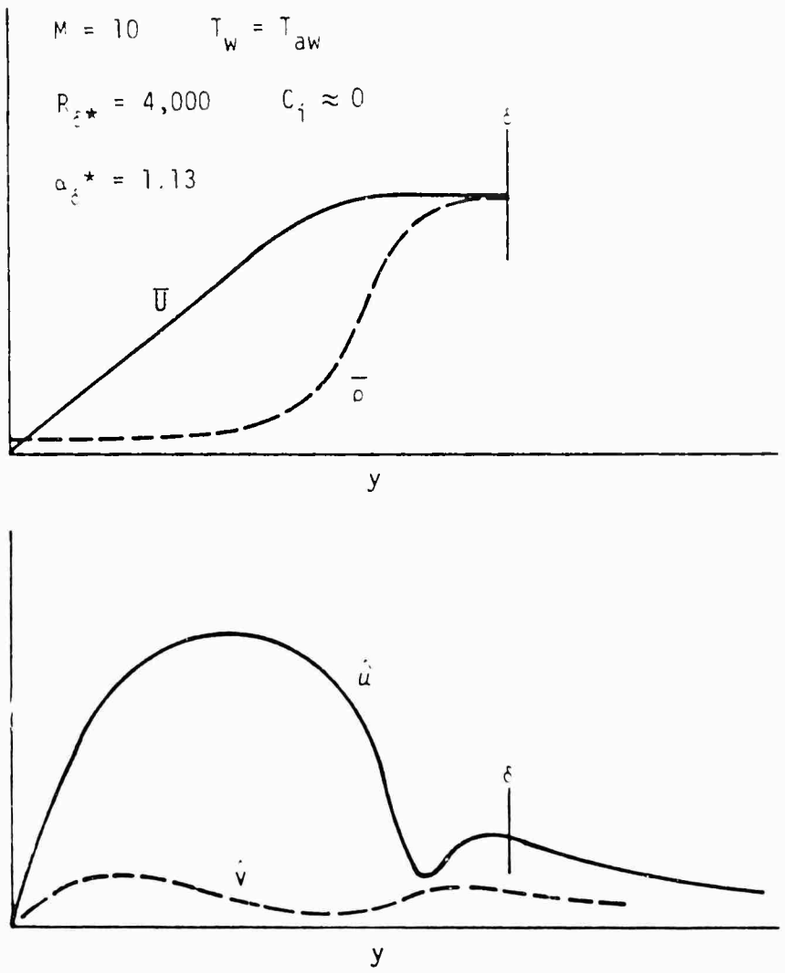

Figure 4. DISTURBANCE PROFILES AT M = 10

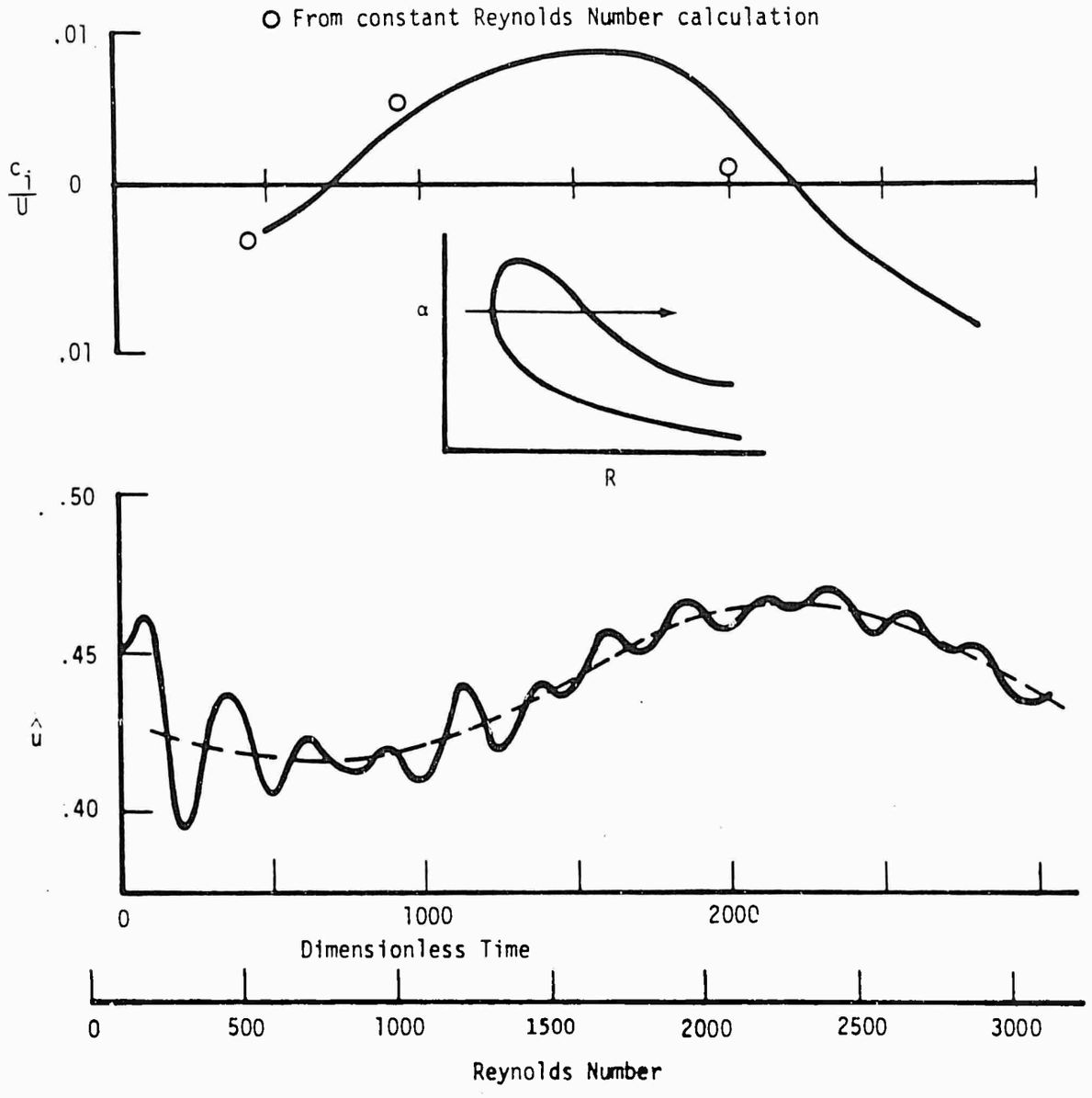

Figure 5. DISTURBANCE AMPLITUDE WITH LINEARLY INCREASING REYNOLDS NUMBER

a consistent set of amplification rates were determined. The values obtained are also shown in Figure 5, where it is seen that they are not greatly different from those obtained from the constant Reynolds number calculations (Figure 3). As might be expected, the varying Reynolds number results lag those obtained at a constant Reynolds number.

It might be suggested that the Reynolds number should have been increased as a square-root function of the time in order to approximate the growth rate of the laminar boundary layer. Such a variation of Reynolds number with time is no more difficult to calculate than the linear variation used here, but would lead to much more rapid changes of Reynolds number at early times, and, it is felt, would yield less accurate results. The linear variation used here should be regarded merely as a mathematical artifice, and not as an attempt to simulate a physical effect.* It should be remarked that the varying Reynolds number calculation involved so little increase in computer time that no accurate determination of the increase could be made.

As a final example of the present method, Figure 6 illustrates a nonlinear effect, namely, the effect of the Reynolds stresses associated with the disturbance waves. The initial boundary layer profile was the Blasius solution. At time zero, an initial disturbance of approximately 40 fps. or about 10% of the freestream velocity was introduced. At the end of the calculation, the profile had distorted into the shape indicated by the solid curve of Figure 6. Although the distortion is slight, the rate of disturbance amplification had increased five-fold, as noted on the figure. As with the variable Reynolds number calculation, no appreciable increase in computer time was caused by the added calculations.

---

*In the case of classical method, Dr. R. C. Gunness, of The Boeing Company, has re-examined the order of magnitude and significance of the streamwise space derivatives which are generally omitted (parallel flow assumption). It was found that the parallel flow assumption is valid only when the spacial amplification rate times the Reynolds number is generally much greater than unity. This conclusion is supported by the experimental data of Laufer (Reference 24) who found a marked dependence of the amplification rates on the normal coordinate. The possibility that an extension of the criteria can be used in the present analysis to estimate the extent of the lag effect (due to the time variation of Reynolds number) is being investigated.

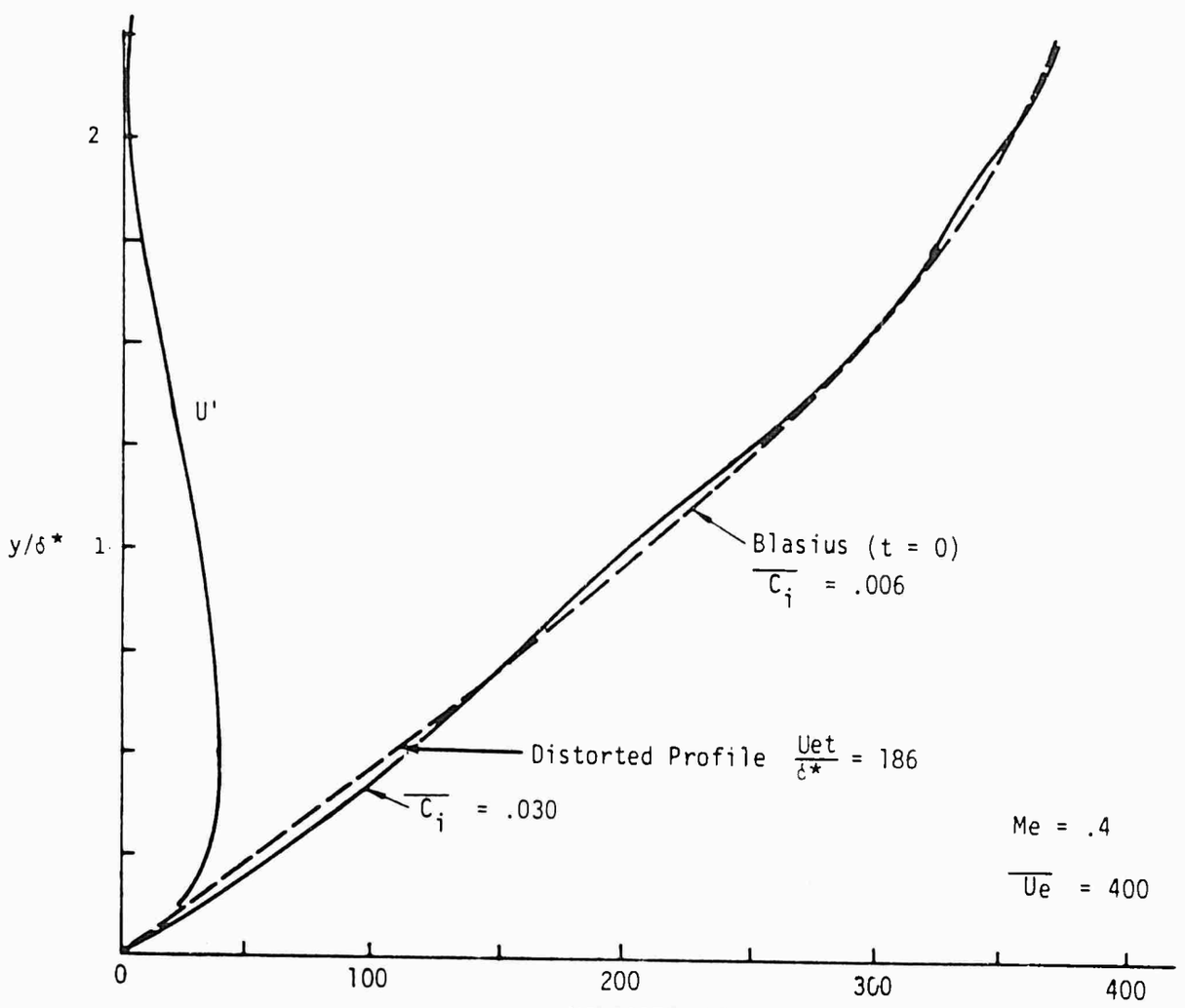

Figure 6. EFFECT OF REYNOLDS STRESS ON MEAN VELOCITY PROFILE AND AMPLIFICATION RATE

Concluding Remarks - Stability Study

The study described here is still in progress. The technique described is not intended so much as a new method for stability calculations as it is the first stage in the development of a transition theory. The calculation of stability is done primarily as a check on the accuracy of the method, and is a very severe test because of the relative smallness of the viscous terms. Indeed, a superficial analysis would suggest that the errors in the inviscid terms would be so large as to completely mask any Reynolds number effects.

For the present purposes of comparison, the equations have been linearized by deleting all terms involving products of perturbations. However, calculations have been made with the full nonlinear equations to verify that the integration technique will work equally well, and all indications are that no further development of a purely numerical nature will be required. However, in the nonlinear calculations that have been made, the nonlinear terms have been small. It is possible that new numerical effects will arise when these terms are made larger. The deletion of the nonlinear terms was found to reduce the computer time by 25 to 35 percent.

Other calculations have been made to verify that the restriction to sinusoidal disturbance waves is not essential to the success of the method. In these calculations, several x-stations were used and the derivative expressions of Eqn. (12) were replaced by central difference formulas. These cases also appear to be working well.

It still is to be determined how far into the transition region the calculation can be extended. The present linearized calculations require about 20 minutes of computer time (UNIVAC 1108) for a single combination of α - Re, beginning from a pulse disturbance (as in Figure 1). This can be reduced to about 10 minutes if the final profiles from a previous calculation are used as initial values. Thus, it may appear that the method has about reached its practical limit. However, it has also been shown that additional physical complexity does not necessarily require large increases in computer time. A preliminary analysis indicates that a three-dimensional calculation of the Benney-Lin type (References 10 through 13) would require only two to four times as much computer time as the present calculations. Such an

increase would not make the calculation infeasible, particularly considering the steady increases in computer speed that has occurred in the past.

As discussed in Benney's papers, the Benney-Lin flow model may be adequate to bridge the gap between the linear stability region and origin of turbulent spots. Beyond that point, the flow is apparently fully turbulent for some fraction of time, and one cannot now foresee the extension of the present technique into even localized regions of turbulence. However, as shown in the second portion of this paper, there is good reason to believe that the transition zone may be amenable to more traditional methods of analysis.

PART II
AN EXTENSION OF EMMONS' TRANSITION THEORY TO HYPERSONIC FLOW

In 1950, Emmons (Reference 3), discovered that subsonic transition began with the appearance of small regions of turbulence ("Emmons Spots") in the laminar flow. The spots, or bursts, were observed to travel downstream at a uniform velocity, increasing in size but preserving their shape. Near the leading edge the spots were widely spaced, and were entirely surrounded by laminar flow Downstream they merged to form a completely turbulent boundary layer. Emmons' sketch illustrating spot behavior is reproduced below:

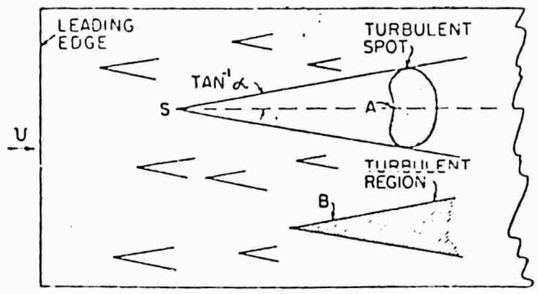

FIG. 4. Transition on a flat plate.

More recent experiments, including those by Schubauer and Klebanoff (Reference 4) and Elder (Reference 5) verified Emmons' observations, and added much detail information. It was shown that spot formation is essentially "pointlike" in the sense that size of the spot is initially of the order of the laminar boundary layer thickness, and it was also found that there are essentially no interaction effects between spots. This latter characteristic insures that the intermittency factor at any point can be calculated by adding the effects of individual spots, a property that is used in the present analysis. The shape and growth rate of the turbulent spots are clearly independent of the Reynolds number, since neither changes as the spot moves downstream.

Turbulent spots have since been observed in supersonic and hypersonic flows. Many shadowgraphs showing bursts at Mach numbers from about 3.7 to 7 are presented by C. S. James in Reference 6. In all cases the turbulent spots appear to travel downstream at a uniform speed, and to grow

laterally at a rate that is also constant, so that the area swept out by any particular spot is a triangular region as Emmons had sketched. James also found that the shape of the turbulent spots was very similar to those observed in subsonic flow. The angle, $\tan^{-1} \alpha$, that defines the zone of influence appears to be nearly independent of Mach number as well, since it was found to be about the same in James' observations at Mach 3.7 as in the subsonic observations -- about 10 degrees. There is some suggestion in James' data that α may decrease at higher Mach numbers, however.

Emmons' and James' observations differ significantly as to the origin of the spots. Emmons observed them forming in the laminar flow well downstream of the leading edge, while James concluded that in his experiments the spots had been formed near the leading edge.

Analysis

In Reference 3 Emmons also formulated a probabilistic theory of transition, assuming that spots are formed randomly within the laminar region. In his theory the boundary layer is considered to be fully turbulent at a point if a spot is present and otherwise completely laminar. Thus, there is no transitional boundary layer as such, only a time-averaging between the laminar and turbulent states. There was not at that time sufficient data to subject Emmons' theory to any quantitative comparisons with experiment. Later, however, Dhawan and Narasimha (Reference 7) showed that the measured distribution of intermittency through the transition region as reported in Reference 4 could be predicted by Emmons' theory, if all spots were assumed to form along a line parallel to the leading edge, rather than throughout the laminar region as Emmons had assumed. They also showed that many of the properties of the boundary layer in the transition region could be calculated by appropriate time-averaging of the laminar and turbulent boundary layers.

The following calculation differs from those of References 3 and 7 only in the assumptions made regarding the formation of turbulent spots. The nomenclature of the analysis is illustrated in the sketch below:

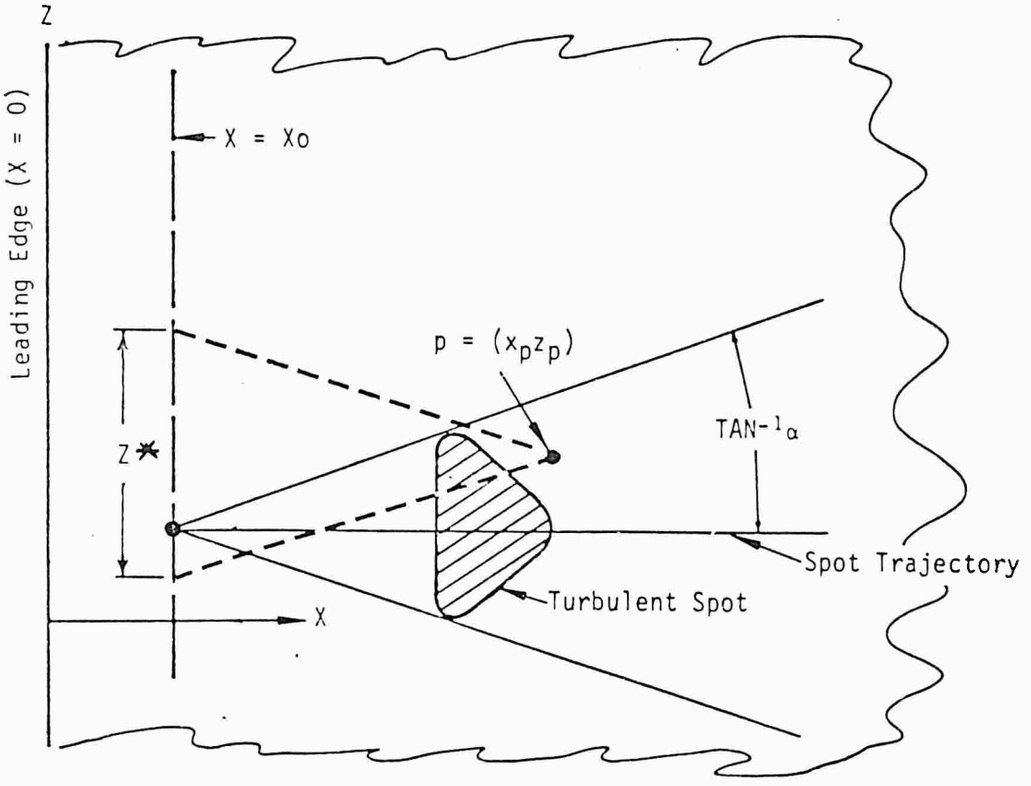

The surface over which the boundary layer develops may be considered as either an unswept flat plate of infinite span or a hollow cylinder aligned with the freestream flow. It is assumed that all spots are formed at a particular value of x, namely x_o. The flow in the region $x < x_o$ is laminar, and, therefore, can be scaled by Reynolds number similarity. Downstream of x_o the assumptions regarding the behavior of turbulent spots determine the results of the analysis. The assumptions used here are the same as those of References 3 and 7, namely, the spot velocity, shape and growth rate are independent of the distance, and in particular, independent of the unit Reynolds number.

Now, let $\gamma(z_1, z_2, p)$ be the fraction of time that the point p is covered by at least one spot formed in the portion of the line $x = x_o$ bounded by z_1 and z_2. As in Reference 3, it is assumed that the spots are entirely

independent, but that if two spots are present at p simultaneously, only the first to arrive is included in calculating γ . These assumptions imply the following relation for γ (provided Δz is small):

$$\gamma(-\infty, z_1+\Delta z, p) = \gamma(-\infty, z_1, p) + \left[1-\gamma(-\infty, z_1, p)\right]\gamma(z_1, z_1+\Delta z, p) \quad (13)$$

which is analagous to Eqn. (2) of Reference 3. Taking the limit as $\Delta z \to 0$ yields:

$$\frac{1}{1-\gamma(-\infty, z_1, p)}\frac{\partial}{\partial z}\left\{\gamma(-\infty, z_1, p)\right\} = \lim_{\Delta z \to 0}\frac{\gamma(z_1, z+\Delta z, p)}{\Delta z} \quad (14)$$

By taking Δz sufficiently small the spacing in time (and hence the spacing in distance) of the spots formed in the region $z_1 < z < z_1 + \Delta z$ can be made sufficiently large that the spots will remain distinct in the region of interest, namely, $x \leqslant x_p$. Then $\gamma(z_1, z_1 + \Delta z, p)$ can be written:

$$\gamma(z_0, z_0+\Delta z, p) = \frac{1}{t_2-t_1}\left[\int_{t_1}^{t_2} f^* \Delta y \left(\frac{x_d - x_u}{c}\right) dt\right] \quad (15)$$

where f* is the instantaneous rate of spot formation per unit z, x_d is value of x_s for which the downstream edge of the spot reaches p, x_u is the value of x_s when the upstream edge of the spot passes over p, and c is the spot velocity dx_s/dt. Since the spot velocity and shape are independent of time, Eqn. (15) can be simplified to:

$$\gamma(z_1, z_1+\Delta z, p) = \left(\frac{x_d - x_u}{c}\right)\left(\overline{f^*}\, dz\right) \quad (16)$$

where $\overline{f^*}$ is the mean spot formation rate, defined by

$$\overline{f^*} = \frac{\int_{t_1}^{t_2} f^* dt}{t_2 - t_1} \quad (17)$$

The mean spot formation rate is assumed to be uniform, in the sense that

$$\frac{\partial \overline{f^*}}{\partial t} = \frac{\partial \overline{f^*}}{\partial z} = 0 \quad (18)$$

With (16) and (18), Eqn. (14) is easily integrated to yield:

$$\gamma(\rho) = 1 - \exp\left\{ \int_{-\infty}^{\infty} \overline{f^*} \left(\frac{x_d - x_u}{c} \right) dz \right\}$$

$$= 1 - \exp\left\{ -\frac{\overline{f^*}}{c} \int_{-\infty}^{\infty} (x_d - x_u)\, dz \right\} \qquad (19)$$

It will be seen that the integral of (19) can be written in terms of a spot shape function, σ , as follows:

$$\int_{-\infty}^{\infty} (x_d - x_u)\, dy = (x_p - x_o)^2 \alpha^2 \int_{-1}^{1} \frac{x_d - x_u}{(x_p - x_o)\alpha} \frac{dz}{(x_p - x_o)\alpha} \qquad (20)$$

$$= (x_p - x_o)^2 \alpha^2 \sigma \qquad (21)$$

where σ now depends only on the shape of the spots. Using (21), and noting that because of (18) there is no dependency of γ on z, (19) can be written as

$$\gamma(x) = 1 - \exp\left\{ -\frac{\overline{f^*}}{c} (x_p - x_o)^2 \alpha^2 \sigma \right\} \qquad (22)$$

It will now be seen that if $\overline{f^*}$ were known, it would be possible to predict transition, since α, c and σ are all known with good accuracy from the Reference 4 experiments. Even though $\overline{f^*}$ is not known explicitly, dimensional analysis leads to the following useful relation:

$$\overline{f^*} = \left(\frac{f U_e^2}{\nu_e} \right) \left(\frac{1}{\lambda_z} \right) \qquad (23)$$

In (23) f is a dimensionless frequency and as such may be a function of any of the usual dimensionless numbers of fluid mechanics. The second factor, λ_z, must have the dimensions of length. It may seem appropriate to select some characteristic model dimension here; however, it will be advantageous not to do so. It can readily be seen that λ_z must, in fact, be a measure of the average spanwise spacing of the turbulent spots, and its relation to other physical quantities will be discussed a little later. Now, combining (22) and (23) yields:

$$\gamma(x) = 1 - \exp\left\{-\left(\frac{f U_e}{\nu_e \lambda_z}\right)\left(\frac{(x_p - x_o)^2 \alpha^2 \sigma}{c}\right)\right\} \tag{24}$$

As in Reference 3, "transition" is defined as the attainment of a particular value of γ . The actual value is immaterial, since the condition $\gamma = \gamma_T$ is sufficient to obtain a transition scaling rule. If x_T is the value of x at which $\gamma = \gamma_T$, then

$$\left(\frac{f U_e}{\nu_e \lambda_z}\right) \frac{(x_T - x_o)^2 \alpha^2 \sigma}{c} = \ln\left(\frac{1}{\gamma_T - 1}\right) = \text{CONST.} \tag{25}$$

from which

$$Re_T - Re_o \equiv \frac{U_e (x_T - x_o)}{\nu_e} = \ln\left(\frac{1}{\gamma_T - 1}\right)\sqrt{\frac{c \lambda_z}{\nu_e \alpha^2 f \sigma}} \tag{26}$$

Eqn. (26) implies the following form for Re_T:

$$Re_T = Re_o + (\text{CONST})\sqrt{\left(\frac{U_e \lambda_z}{\nu_e}\right)\left(\frac{c}{U_e}\right)\frac{1}{\alpha^2 f \sigma}} \tag{27}$$

According to (27), it will be seen that Re_T will be constant only if the Reynolds number based on λ_z is constant.

Available Information for λ_z

The lateral scale length λ_z is a measure of the relative importance of three-dimensional effects in transition; if λ_z is small, the flow must be highly three-dimensional. Although there has been some controversy over the interpretation of experimental results, there is general agreement that the flow becomes highly three-dimensional prior to the appearance of turbulent spots. In the experiments of Reference 8, for example, it was found that both the "steady" boundary layer and the Tollmien-Schlichting disturbance waves possessed a spanwise periodicity with more or less regularly spaced "peaks" and "valleys". It was noted that turbulent spots were created

only at the peaks, and never at the valleys. Hence, the spacing of the peaks can be identified with the lateral spacing parameter, λ_z , of the present analysis.

The factors that determined the spacing of the peaks and valleys in those experiments could not be clearly identified, however. Attempts to determine these factors are described in Reference 8, including varying the Reynolds number, changing the plate angle-of-attack, refinishing, and finally entirely resurfacing the plate, without causing significant changes in the locations of the peaks. It was also shown that the effect was not due to the vibrating string mechanism that was used to initiate Tollmien-Schlichting waves in some of the experiments. The only factor found to affect the peaks and valleys was the turbulence-reducing screen system ahead of the test section. Cleaning these screens was found to alter the location, but not the spacing, of the peaks. In a later study, Klebanoff, Tidstrom and Sargent (Reference 9) concluded that the three-dimensional behavior is an authentic characteristic of transition, and not to be attributed to deficiencies in previous experimental techniques.

Some theoretical studies of three-dimensional effects have been made, one of the earliest and most far-reaching being a theorem by Squire (Reference 23) to the effect that linear three-dimensional disturbances in an incompressible boundary layer are more stable than two-dimensional disturbances. Nonlinear three-dimensional analyses have been made by Benney and his colleagues (References 10 through 13) that consider the interaction of two-dimensional disturbance waves with vortices whose filaments are parallel to the freestream. The complexity of the mathematics involved has necessitated a number of simplifying assumptions regarding the flow field, and the analysis is limited to incompressible flows. Nevertheless, the calculated results show many points of similarity to the experimental results of Reference 9, suggesting that the most important physical processes (for low speeds, at least) may be those considered by the theory. For this reason, it is perhaps highly significant that the theory does not yield a critical spacing for the streamwise vortices. The failure of the theory to identify

a critical lateral spacing suggests that the spacing is not determined by the stability equations, but is somehow imposed by the boundary conditions, either at the model or in the freestream. Since the Reference 8 experiments eliminated the model as the source of the preferred spacing, some effect of the testing facility is indicated. The facility of course exerts a major influence through the characteristics of the flow it provides, and it is well known that turbulence always exists in wind-tunnel flows. Turbulence is characterized not only by its intensity, but also by a characteristic length, the turbulence scale, which is a measure of the size of the turbulent eddies. The existence of a characteristic length in both the freestream flow and in the boundary layer suggests that the two are somehow related. Indeed, since the Tollmien-Schlichting waves are often initiated by freestream turbulence, it would be expected that these waves would exhibit spanwise variations in amplitude, more or less proportional to the spanwise variations in the intensity of the initial disturbances. The apparent insensitivity of the peak and valley spacing to flow conditions is consistent with the conjectured relation between λ_z and the freestream turbulence scale, since turbulence scale tends to depend on the physical dimensions of the flow field rather than on its velocity or density.

The Unit Reynolds Number Effect

If it is assumed that λ_z is proportional to the freestream turbulence scale, which is in turn assumed to be independent of the flow conditions, it will be seen that Eqn. (27) requires Re_T to increase with the unit Reynolds number $\frac{U_e}{\nu_e}$. The effect will be small in the usual subsonic experimental conditions, however. In the experiments of Reference 4, for example, Re_o was found to be about 3×10^6, and transition was complete at a Reynolds number of about 4×10^6. If x_T is defined at the mid-point of the transition region, then $Re_T - Re_o$ is only about 5×10^5, and that according to Eqn. (27) doubling the unit Reynolds number would produce only about 5 percent change in Re_T. It is not surprising that the unit Reynolds number has not been recognized as a necessary parameter in correlating subsonic transition data.

Laufer, in Reference 14, has shown that in a supersonic wind tunnel, the freestream turbulence is almost entirely due to disturbances radiated from turbulent boundary layers on the tunnel walls. This observation allows a theoretical estimate of the λ_z, assuming again that λ_z is determined by the tunnel turbulence scale, since the turbulence scale of the turbulent boundary layer should be proportional to the boundary layer thickness. Thus, λ_z will be proportional to $\delta_{B.L.}$, the boundary layer thickness, which, according to turbulent boundary layer formulas, scales as

$$\delta_{B.L.} \sim D(Re_D)^{-.2} \tag{28}$$

Taking λ_z proportional to $\delta_{B.L.}$, Eqn. (27) becomes

$$Re_T \equiv \frac{U_e x_T}{\nu_e} = \left(\frac{U_e x_o}{\nu_e}\right) + (\text{CONST})\sqrt{\left(\frac{U_e D}{\nu_e}\right)^{.8} \frac{c}{U_e f \alpha^2 \sigma}} \tag{29}$$

Eqn. (29) appears to have an even weaker dependency on the tunnel diameter Reynolds number than in subsonic flows. However, in the hypersonic experiments of Reference 6, turbulent spots were observed forming a local Reynolds number of only 0.5×10^6 to 1.0×10^6, while transition data from similar experiments (Reference 5) show that transition occurs at Reynolds numbers of 8×10^6 to 15×10^6. The relative magnitudes of x_o and x_T implied by these data indicates that the first term of Eqn. (29) is negligible, and Re_T will vary strongly with the tunnel diameter Reynolds number. Numerical calculations show that for the case just described, the second term of (29) may be neglected entirely, leading to

$$Re_T \sim \left(\frac{U_e D}{\nu_e}\right)^{.4} \sqrt{\left(\frac{c}{U_e}\right) \frac{1}{f \alpha^2 \sigma}} \tag{30}$$

There being no variation of c/U_e, f, α or σ with unit Reynolds number, Eqn. (30) predicts an apparent "unit Reynolds number effect" in natural transition data from any particular wind tunnel.

A strong unit Reynolds number effect has in fact been observed in many experiments, involving many different wind tunnels and model geometries.

Representative boundary layer transition data for flow-aligned hollow cylinders are plotted in Figure 7 as a function of the unit Reynolds number. By comparing the slopes of the data curves with that given by the theory, it is seen that Eqn. (30) is in good agreement with the experimental unit Reynolds number effect.

Some additional data, including some for other geometries, are presented in Figure 8. This figure is taken from Reference 15, and is unaltered except for the addition of the theory curve. Again, it is seen that the unit Reynolds number trend is well predicted.

According to the present analysis, confirmed by experimental results, the dimensionless group

$$\overline{Re}_T = Re_T/(Re_D)^{.4} \qquad (31)$$

is the proper correlating parameter for boundary layer transition data from hypersonic wind tunnels, and this parameter will be used for the remaining comparisons. $\overline{Re}_T$ cannot be expected to provide exact agreement between data from different wind tunnels unless the tunnels themselves are geometrically similar. The disturbances that actually cause transition on the model may originate upstream of the test section, and so will be affected by the angle of nozzle divergence, for example.

Two sets of directly comparable data are presented in Reference 16, however, wherein the same model was used in two similar wind tunnels of different sizes. The data were obtained at a Mach number of 4, and are for the point of maximum surface pitot pressure. It is shown in Figure 9 that the two sets of data are brought into excellent agreement by the use of $\overline{Re}_T$, and further, that the experimental value of $\overline{Re}_T$ is independent of the unit Reynolds number. By comparing Figure 9 with the final figure it will be seen that $\overline{Re}_T$ may also provide good agreement of data from different facilities, a fortunate result which may be ascribed to the insensitivity of turbulent boundary layers to the effects of geometry and pressure gradients.

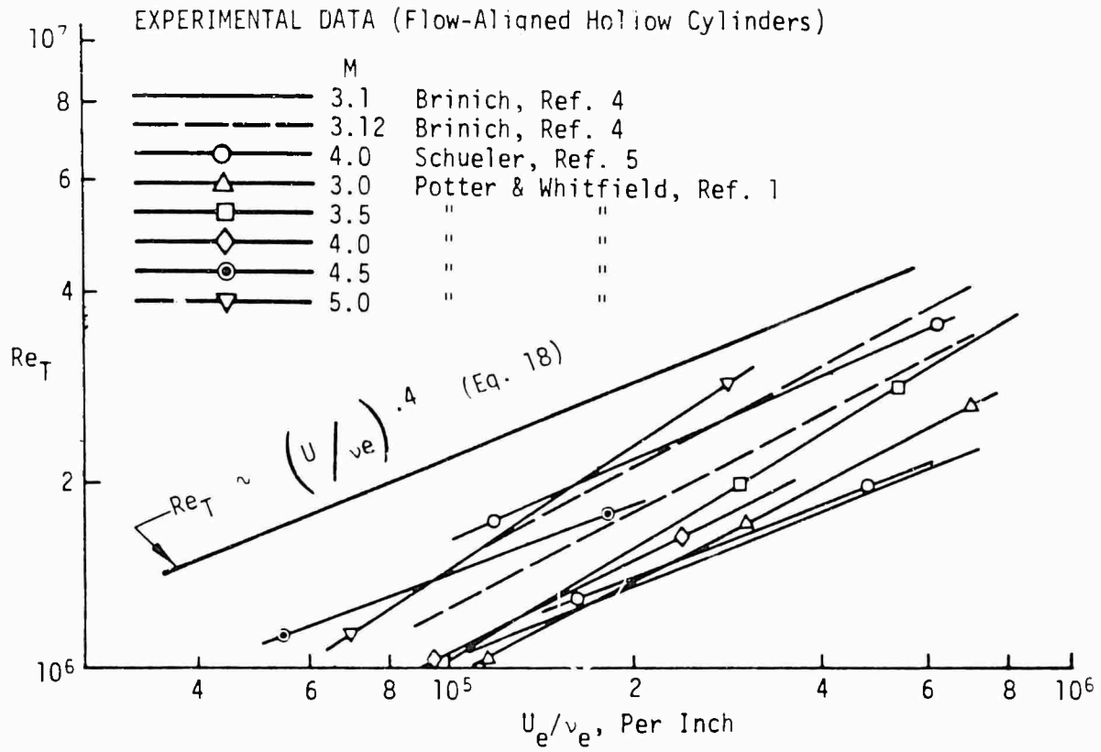

Figure 7. EFFECT OF UNIT REYNOLDS NUMBER ON TRANSITION

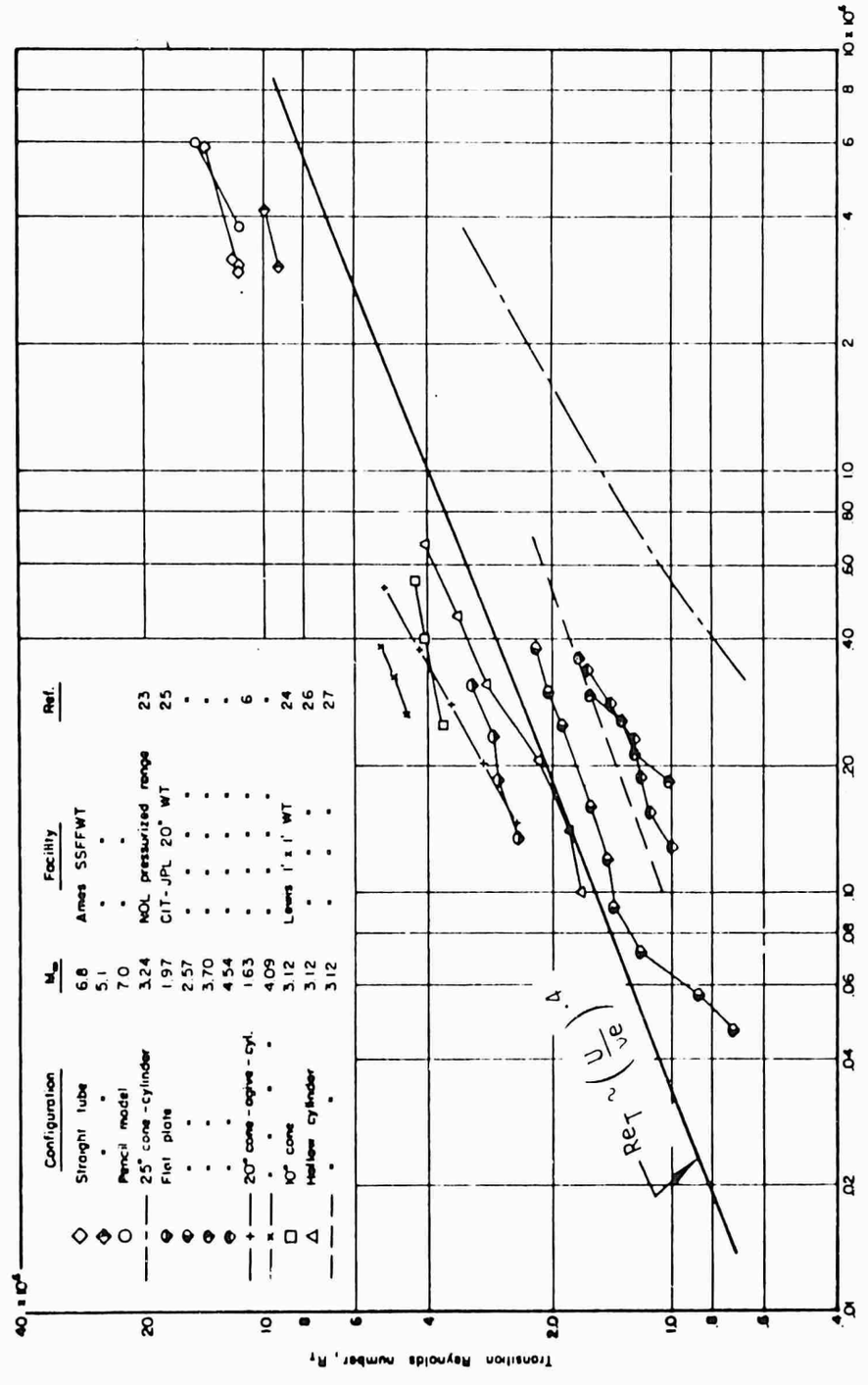

Figure 17.- Variation of transition Reynolds number with unit Reynolds number on surfaces having subcritical roughness.

Figure 8. TRANSITION REYNOLDS NUMBER COMPARISON FROM REFERENCE 15

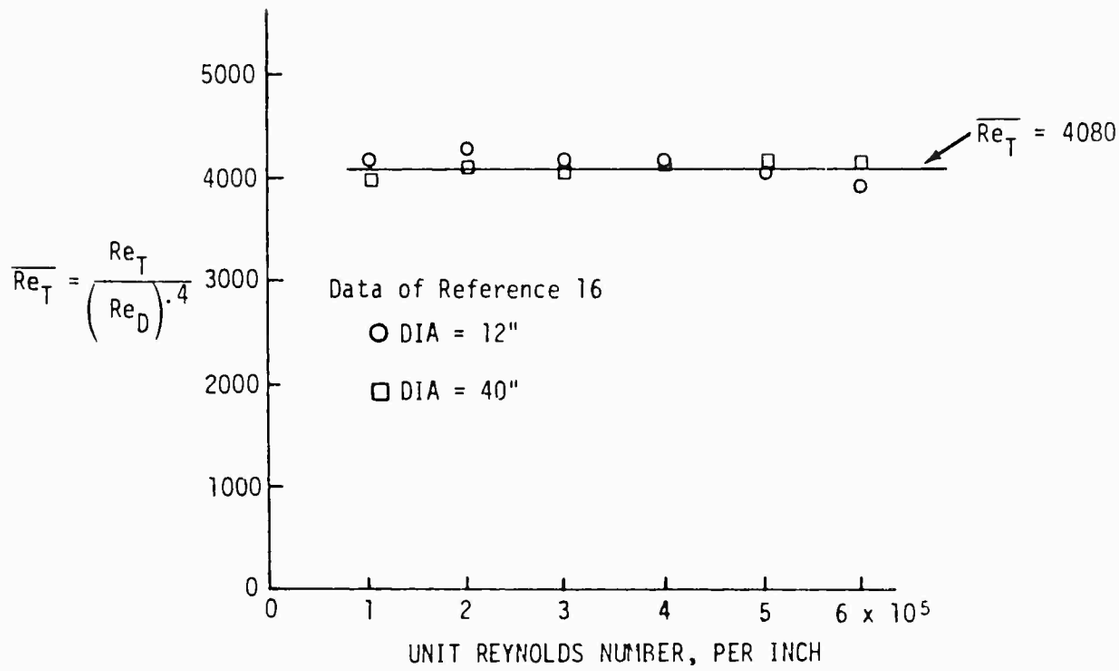

Figure 9. CORRELATION OF TRANSITION DATA FROM TWO WIND TUNNELS

Effect of Leading Edge Sweep

The calculation described in the previous section has been extended to the case of a swept, two-dimensional flat plate, assuming that the local flow direction remains parallel to that in the freestream, with the result that the variation of Re_T with Re_D is predicted to be independent of sweep. Therefore, $Re_T/(Re_D)^{.4}$ should serve as a correlating parameter for swept plate data as well. The experimental results of Reference 17 confirm this conclusion, as is shown in Figure 10. The two sets of data shown are for the points of minimum and maximum surface pitot pressure as determined by a streamwise survey with a moving probe as near to the surface as the equipment will allow. The scatter in the correlated data is scarcely greater than that in the original data at a given unit Reynolds number, as may be seen by examining the data for individual conditions.

To calculate the effect of sweep on the transition Reynolds number, further information is required. The dimensionless frequency f may vary with sweep, and the spots may become asymmetrical or the angle α may be altered. Unfortunately, no data are available regarding these possible effects. However, if it is assumed that sweep has no effect on f, α or the other quantities entering into (29), the calculated sweep effect is:

$$\frac{Re_{T,\Lambda}}{Re_{T,\Lambda=0}} = \sqrt{(1-\alpha^2\tan^2\Lambda)\cos\Lambda} \qquad (32)$$

Eqn. (32) is relatively independent of either α or σ for sweep angles less than about 60 degrees. For the present comparisons α is assumed to be 10 degrees, the value assumed by Emmons, although there is some reason to believe that α is somewhat less at the Mach number of this comparison. For $\Lambda < 57$ degrees, it is estimated that the maximum effect of σ will be less than 5 percent increasing to about 20 percent at $\Lambda = 75$ degrees. In that same range a change in α of 2 degrees would produce about the same changes. Of course, Eqn. (32) breaks down entirely for $\alpha \geq 90 - \Lambda$.

Eqn. (32) is plotted in Figure 10 with the questionable portion indicated by dashes. It is seen that the data agree very well with the beginning transition for sweep angles up to about 60 degrees. The end transition data are consistently above the theory, however. It is, of course, entirely possible that the assumptions in the theory are not satisfied by the flow over a swept plate. However, it will be seen from the geometric information given in

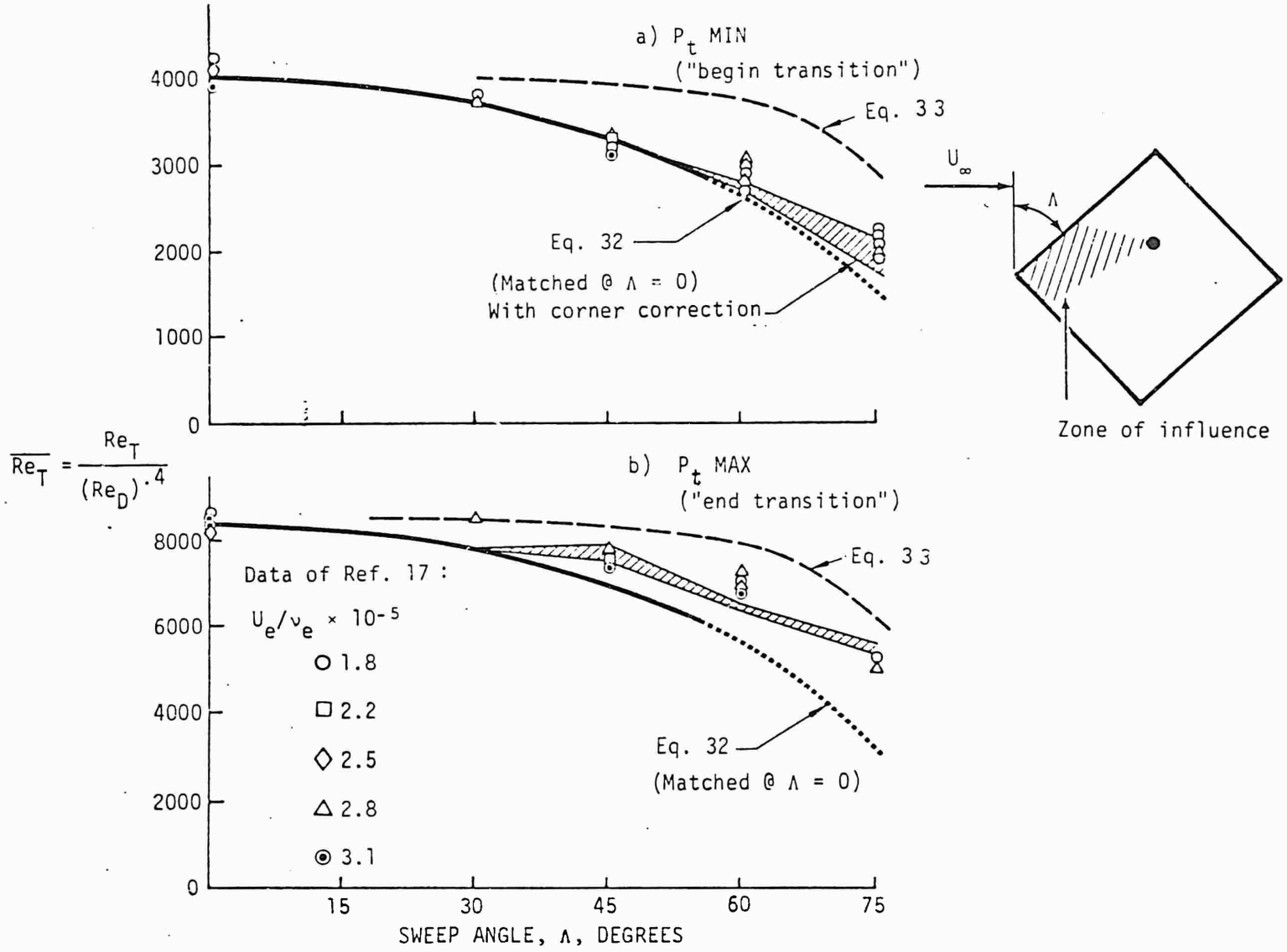

Figure 10. EFFECT OF LEADING EDGE SWEEP ON FLAT PLATE BOUNDARY LAYER TRANSITION; M = 8.1, T_w = 9 Taw.

Reference 17 that the "swept plate" was actually a rotated square plate. According to the present theory, most of the data would be affected by the corners of the plate, with the greatest effect at the lowest unit Reynolds and for the "end transition" data. The amount of the correction depends on the shape of the turbulent spots and the location of the pitot probe with respect to the corner. Neither are known with accuracy, but an approximate calculation of the corner effect has been made which is shown by the shading in Figure 10. It is seen that the agreement is greatly improved. It is emphasized that the corner effect calculation is only a correction for the difference in model planform between that actually used in Reference 17 and the ideal, two-dimensional swept planform assumed in deriving Eqn. (32)

It should also be noted that Eqn. (32) assumes that the number of spots produced depends on the actual slant length of the leading edge rather than the projected length. The latter assumption leads to*

$$\frac{Re_{T,\Lambda}}{Re_{T,\Lambda=0}} = \sqrt{1 - \alpha^2 \tan^2 \Lambda} \qquad (33)$$

Eqn. (33) is also shown in Figure 10. Even without a correction for the corner effect, it is seen that Eqn. (33) predicts far too little reduction in Re_T with sweep.

Spot Production Rate and Stability Theory

There is some reason to believe that the spot production rate will be related to the critical frequency given by stability theory. Subsonic experiments have followed the growth of instability waves until their breakdown, and that waves of the Tollmien-Schlichting type have been found to exist until just before turbulence appears. Benney and Greenspan (Reference 12), on the basis of theoretical calculations and the experimental results of Klebanoff, Tidstrom and Sargent (Reference 9) believe that a breakdown to turbulence will occur once each cycle of the Tollmien-Schlichting waves. If this is so, the spot production rate will be proportional to that of the

*Eqn. (33) was also obtained by Emmons and Bryson in Reference 18.

Tollmien-Schlichting wave most unstable with respect to the breakdown process. There is at present no way to determine this most unstable frequency, but, in general, the unstable frequencies given by boundary layer stability theory decrease strongly with Mach number at hypersonic speeds. Lees and Reshotko (Reference 19) give an asymptotic rule for the most unstable frequency at high Mach numbers that may be written (in the present notation)

$$f \sim \frac{1}{M^2} \tag{34}$$

This rule assumes that the viscosity is proportional to the temperature. A more complete calculation by Mack (Reference 20) gives results for the most highly amplified disturbance frequency for the limiting case of infinitely large Reynolds numbers. Mack's numerical results are well represented by

$$f \sim \frac{1}{M^{1.75}} \tag{35}$$

in the range of Mach numbers from 4 to 10.

Inserted into Eqn. (30), (34) implies a linear increase in transition Reynolds number with Mach number, while (35) leads to

$$Re_T \sim M^{.875} \tag{36}$$

Relation (35) will be used in the following comparisons because it is based on more complete calculations, although it will be seen that use of (34) would yield slightly better correlations. Several other effects of Mach number may be anticipated, including an increase in c/U (which was observed in Reference 6), an increase in tunnel wall boundary layer thickness, and possible effects on α and σ. No attempt to include these effects will be made, however. There are no definitive data on which to base such calculations, and it will be seen that the frequency effect is probably the largest single factor in the present range of interest.

Experimental data from References 1 and 17 are compared with the predicted Mach number effect in Figure 11. The data are taken from three

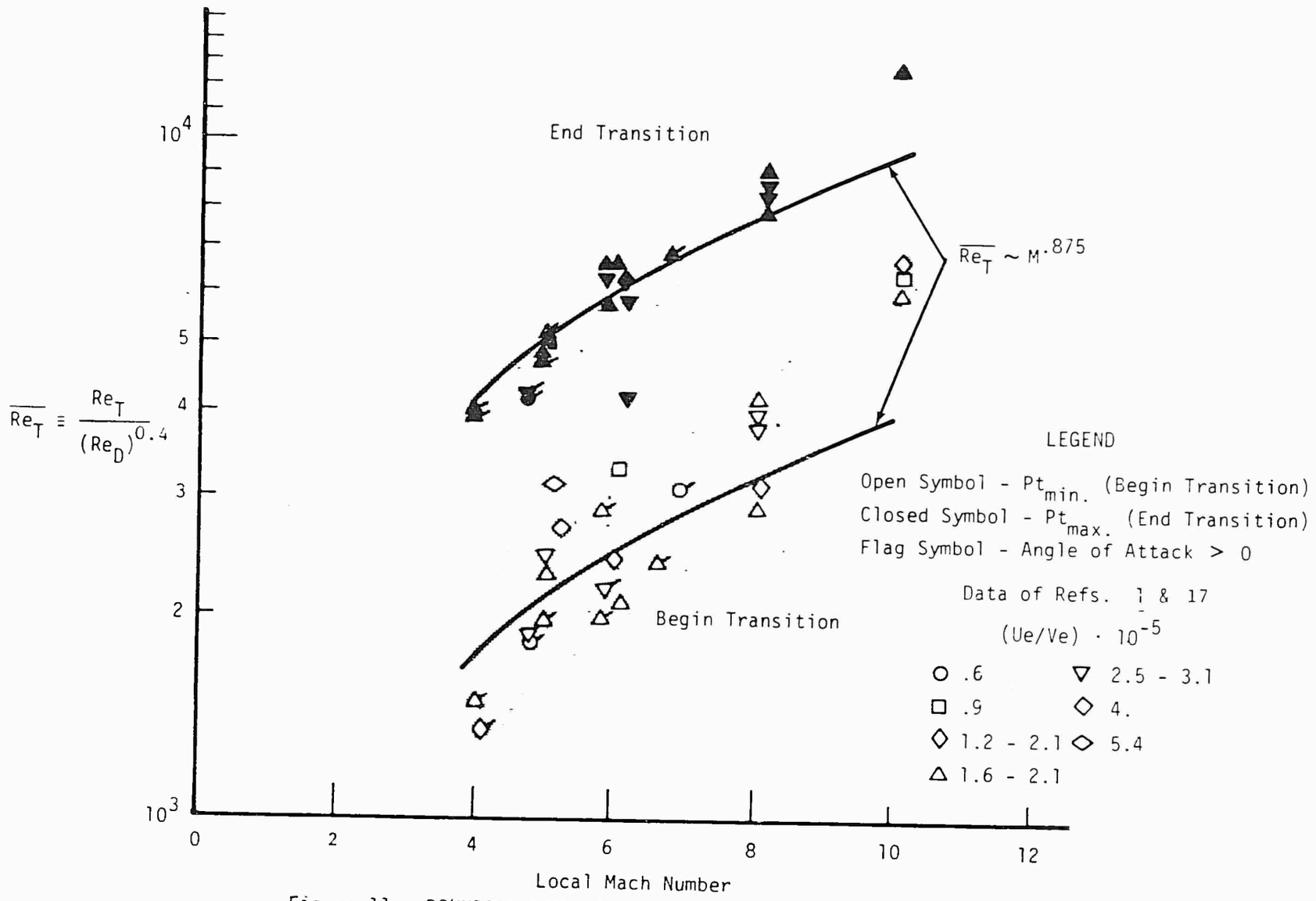

Figure 11. BOUNDARY LAYER TRANSITION ON SHARP FLAT PLATES

different wind tunnels and for four different freestream Mach numbers. By varying the angle-of-attack from zero to 15 degrees, the local Mach number range in the Reference 1 tests was extended down to about 3.95. The data shown are for nominally sharp leading-edge models; the leading-edge diameter of the Reference 1 model was about .001 in. and that of the Reference 17 model was about .002 in. Data are given in both references for the "beginning" and "end" of transition as previously defined.

As may be seen in Figure 11, the proposed correlation parameter groups the end of transition data closely over a range of unit Reynolds numbers of almost an order of magnitude. The beginning transition data show much more scatter, but, as in Figure 10, it will be seen that much of the scatter is present in the original data at a given unit Reynolds number, and is not due to poor correlation of the data for the various unit Reynolds numbers.

Both sets of data exhibit a consistent increase with Mach number that is in good agreement with the predicted Mach number effect up to a Mach number of about 8. At Mach 10, however, the data are well above the prediction. In view of the close agreement for Mach numbers from 4 to 8, it appears that some additional effect may be present in the Mach 10 data. The increase in c/U, as estimated from the data of Reference 6 would increase the predicted Mach number effect by only about 10 percent at Mach 10. The use of (34) rather than (35) in deriving (36) would also increase the prediction by about 10 percent, and so further improve the agreement. However, (35) seems preferable to (34) on theoretical grounds, and it is felt that another explanation for the discrepancy at Mach 10 is required.

The difference could be attributed to the differences of individual wind tunnels, since only one of the three tunnels could produce Mach 10 flow. However, data were taken in the Mach 10 tunnel at 10 degrees angle-of-attack are in agreement with the data from the other tunnels for the same local Mach number (Reference 1), indicating that the discrepancy at Mach 10 is an authentic Mach number effect, and not due to wind-tunnel differences. A possible explanation is that the characteristic spreading angle, $\tan^{-1} \alpha$, is decreased at very high Mach numbers. Such a reduction does not seem unreasonable, but no experimental support for this conjecture is available.

Other Experimental Results

The quantity of experimental data shown in this paper is relatively limited, and deliberately so. First, only data from flat plates or hollow cylinders having sharp leading edges are considered. This restriction seems necessary since the assumptions made regarding turbulent spots are based on observations for those geometries. Some elementary considerations indicate that the assumptions used here may not apply to cones, for example, as noted in Reference 18.

Second, only data from conventional wind tunnels is considered. In very short duration experiments, as are conducted in ballistic ranges, it is felt that vibrations induced by the starting or launching process may affect the data. Also, the effects of roughness may be important on the small models usually used in ballistic range experiments. This is not to say that such effects are present, merely that some question exists. In fact, data from both types of facilities exist that support the results given here.

A third restriction has been imposed, namely, that the data shown are obtained by the surface pitot pressure method. It is known that the various methods of observing transition do not all yield identical values. It is of course possible that the differences between transition Reynolds numbers given by the various methods may be a function of the flow conditions, which would perhaps lead to spurious trends.

The quality of reporting is also a criterion for data selection. In all too many cases, the author merely presents "transition Reynolds numbers" without specifying just what point in the transition zone he thought he was measuring. Only broad trends can be obtained from such reports.

The amount of data meeting all these requirements is rather limited, particularly for Mach numbers greater than 4, the approximate lower limit of the present comparisons. The author has, of course, reviewed much data not meeting all these conditions, and generally, the same trends have been observed. Some of these comparisons are given in Reference 1. The comparisons presented here include all of the applicable data from the reference reports, even to the very low "end transition" point at Mach 6, shown in Figure 11, which is a very suspicious looking point, to say the least.

Concluding Remarks - Transition Theory

It has been shown that some of the observed trends in hypersonic boundary layer transition are predicted by a heuristic theory of the type originally formulated by Emmons in Reference 3. Although the theory is semi-empirical, the assumptions employed in its development are not based on the experimental data to which it is finally compared. It will be recalled that each of the assumptions is based on either direct observations of turbulent spots, wind tunnel noise experiments or stability theory. Thus the rather good predictions that have been obtained are very encouraging, since a certain consistency of transition phenomena over a wide speed range seems to be implied.

The extension of the theory to geometries other than those considered here is easily possible, but the results of such calculations will depend strongly on the assumptions that are made regarding the effect of geometry on the properties of turbulent spots. There are a sufficient number of variables appearing in Eqn. (27) that could be adjusted so that good agreement with experimental results could be obtained, but it seems preferable to await some definitive observations of turbulent spots or some theoretical treatment of the turbulent spots. However, it seems likely that rules derived here may apply to more general situations than those assumed. For example, experimental results have shown that there is a unit Reynolds number effect of approximately the magnitude predicted here in transition data obtained from both boundary layers and wakes generated by cones in hypersonic flight. Also, the Mach number trend of the data shown in Figure 11 closely parallels that observed in wake data, as shown in Reference 1.

It has, of course, previously been suggested that the unit Reynolds number effect was somehow related to external disturbances, although no quantitative rule has been derived, to the author's knowledge. If it is assumed that the unit Reynolds number effect is caused by variations in turbulent intensity, it is then necessary to assume that the boundary layer becomes very stable at high Mach numbers, since it has been shown experimentally that the intensity of freestream disturbances increases rapidly with Mach number. However, it seems that this line of thought cannot explain

the data of Reference 1 (quoted in Figure 11) which shows that the data from all angles-of-attack fall onto a single curve when plotted as a function of local Mach number and local Reynolds number. Rather, one would expect that at a given local Mach number the transition Reynolds number would decrease with increases in freestream Mach number, due to the increase in the intensity of the external disturbances. No such difficulty arises in the present theory.

A further difficulty with the tunnel noise explanation of the unit Reynolds number effect is the existence of the effect in ballistic range data where there is no external noise. In the present theory, it becomes necessary to discover how λ_z is determined for the ballistic range experiments. In the absence of any other obvious characteristic length, it is suggested that perhaps λ_z is determined by the model size or by surface roughness. Surface roughness may seem like the most likely candidate, since one can visualize a stream of spots emanating from a roughness element. There are, however, experiments indicating that roughness has very little effect at hypersonic speeds. Considering the violent conditions of model launching in a ballistic range experiment, it seems possible that the model may vibrate during the entire experiment and that this vibration may be the source of the initial disturbance that causes transition to occur. In that case, λ_z could be determined by the mode shapes of the vibrating model, which, for a given model, would be the same for an entire series of experiments. According to Eqn. (27) then, the transition Reynolds number would increase as the square root of the unit Reynolds number (provided that $x_o << x_T$, as before). In fact, such a trend has been observed in cone experiments, but this cannot be taken as confirmation of the present analysis due to the geometric differences. However, the relation of λ_z to body size can, perhaps, explain some of the discrepency between rocket experiments and ballistic range data (see References 6 and 25, for example). If the condition $x_o \ll x_T$ is not satisfied in flight, the effect of unit Reynolds numbers would be less than the square root variation since the first term in Eqn. (29) would no longer be negligible.

If λ_z is determined by surface roughness, then it is not clear what effect the unit Reynolds number will have. Increasing the unit Reynolds

number will thin the boundary layer and may actually reduce the transition Reynolds number. If the roughness elements are sufficiently large, however, the location of transition may be fixed independently of the Reynolds number. In this event, the transition Reynolds number would vary linearly with the unit Reynolds number. One would expect that roughness effects are most important in ballistic range experiments where the models are usually small and the unit Reynolds number is often rather large. Some combination of the various effects discussed here may explain the relatively large unit Reynolds number effect shown by the ballistic range data of Figure 8.

Finally, the present analysis suggests a somewhat different relation between stability theory and transition than that usually assumed. According to the final comparison given, one expects transition to be related to the critical frequency rather than the critical Reynolds number. Further investigation is clearly necessary, which, ideally, would consist of direct measurements of the frequency of spot formation.

REFERENCES

1. Nagel, A. L., Savage, R. T. and Wanner, R., "Investigation of Boundary Layer Transition in Hypersonic Flow at Angle of Attack," AFFDL-TR-66-122, August 1964.

2. Kurtz, E. F. and Crandall, S. H., "Computer-Aided Analysis of Hydrodynamic Stability," Jour. of Math. and Phys., Vol. 41, pp. 264-279, 1962.

3. Emmons, H. W., "The Laminar-Turbulent Transition in a Boundary Layer," J. Aero. Sci., July 1951.

4. Schubauer, G. B. and Klebanoff, P. S., "Contributions to the Mechanics of Boundary Layer Transition," NACA TN 3489, 1955.

5. Elder, J. W., "An Experimental Investigation of Turbulent Spots and Breakdown to Turbulence," J. Fluid Mech. 9, (1960).

6. James, C. S., "Observations of Turbulent-Burst Geometry and Growth in Supersonic Flow," NACA TN 4235, April 1958.

7. Dhawan, S. and Narasimha, R., "Some Properties of Boundary Layer Flow During the Transition from Laminar to Turbulent Motion," J. of Fluid Mech. 3, 418 (1958).

8. Klebanoff, P. S. and Tidstrom, K. D., "Evolution of Amplified Waves Leading to Transition in A Boundary Layer with Zero Pressure Gradient," NASA TN D-195, 1958.

9. Klebanoff, P. S., Tidstrom, K. D. and Sargent, L. M., "The Three-Dimensional Nature of Boundary-Layer Instability," J. Fluid Mech. 12, 1 (1962).

10. Benney, D. J. and Lin, C. C., "On the Secondary Motion Induced by Oscillations in Shear Flow," Phys. of Fluids 3, 656-657 (1960).

11. Benney, D. J., "A Nonlinear Theory for Oscillations in a Parallel Flow," J. Fluid Mech. 10, 209-236 (1961).

12. Greenspan, H. P. and Benney, D. C., "On Shear-Layer Instability, Breakdown and Transition," J. of Fluid Mech. 15, 133 (1963).

13. Benney, D. G., "Finite Amplitude Effects in an Unstable Laminar Boundary Layer," Physics of Fluids 7, 319 (1964).

14. Lauer, J., "Aerodynamic Noise in Supersonic Wind Tunnels," J. of Aerospace Sciences, Vol. 28, No. 9, Sept. 1961.

15. James, C. S., "Boundary-Layer Transition on Hollow Cylinders in Supersonic Free Flight as Affected by Mach Number and a Screwthread Type of Surface Roughness," NASA Memo 1-20-59a, February 1959.

16. Schueler, C. J., "A Comparison of Transition Reynolds Numbers from 12-in. and 40-in. Supersonic Tunnels," AEDC-TDR-63-57, March 1963.

17. Deem, R. E. Erickson, C. R. and Murphy, J. S., "Flat-Plate Boundary-Layer Transition at Hypersonic Speeds," Technical Documentary Report FDL-TDR-64-129, October 1964.

18. Emmons, H. W. and Bryson, A. E., "The Laminar-Turbulent Transition in a Boundary Layer," Proceedings of the First U.S. National Congress of Theoretical and Applied Mechanics, June 11-16, 1951, American Society of Mechanical Engineers, New York, N.Y., 1952.

19. Lees, L. and Reshotko, E., "Stability of the Compressible Laminar Boundary Layer," J. of Fluid Mech., Vol. 12, Part 4, April 1962.

20. Mack, L. M., "The Stability of the Compressible Laminar Boundary Layer According to a Direct Numerical Solution," AGARD Specialists Meeting "Recent Developments in Boundary Layer Research," Naples, Italy, May 10-14, 1965.

21. Brinich, P. F. and Sands, N., "Effect of Bluntness on Transition for a Cone and a Hollow Cylinder at Mach 3.1," NACA TN 3979, May 1957.

22. Potter, J. L. and Whitfield, J. D., "Effects of Unit Reynolds Number, Nose Bluntness, and Roughness on Boundary Layer Transition," AGARD Report No. 256, April 1960, 77 p.

23. Squire, H. B., "On the Stability of the Three-Dimensional Disturbances of Viscous Flow Between Parallel Walls," Proc. Roy. Soc., Ser. A., Vol. 142, pp. 621-628, 1933.

24. Laufer, J. and Vrebalovich, T., "Stability and Transition of a Supersonic Laminar Boundary Layer on an Insulated Flat Plate," Jour. Fluid Mech., Vol. 9, Part 2, 1960, pp. 257-294.

25. Rumsey, C. B. and Lee, D. B., "Measurements of Aerodynamic Heat Transfer and Boundary-Layer Transition on a 10° Cone in Free Light at Supersonic Mach Numbers up to 5.9," NASA TN D-745

APPENDIX: NOMENCLATURE

c	velocity of turbulent spot
C_p	specific heat at constant pressure
D	wind tunnel diameter
f	dimensionless frequency (Eqn. 23)
$\bar{f}^*$	frequency of spot formation
H	total enthalpy
m	an integer
n	an integer; degree of polynomial; time level (see Table II)
p	a point
P	pressure
Q_i	general symbol for flow property, ρ , u, v, etc.
R	gas constant
R_e	Reynolds number
$\bar{R}e_T$	normalized transition Reynolds number (Eqn. 31)
t	time
T	temperature
u, v	velocity components
x, y, z	cartesian coordinates
x_o	phase angle (see Eqn. 11); point of formation of turbulent spot
Z^*	width of zone of influence
α	wave number $2\pi / \lambda$; spot growth angle
γ	specific heat ratio; intermittency factor
$\delta_{B.L.}$	tunnel wall boundary layer thickness
δ^*	boundary layer displacement thickness (as in Δx) increment
λ	wavelength
λ_z	characteristic length in Eqn. 23
Λ	leading edge sweep angle
μ	viscosity
ν	kinematic viscosity
ρ	density
σ	spot shape factor
τ	dimensionless time $\left(2t/\Delta y\right)\sqrt{\gamma RT}$
$\bar{\tau}$	dimensionless time $\left(\bar{u}_e t / \delta^*\right)$

Subscripts

aw	adiabatic wall value
d	value of x for which turbulent spot reaches p
D	based on tunnel diameter
e	boundary layer edge value
max	maximum value
N	y-index at last layer for which equations of Table I are computed
p	value at p
s	spot
T	value at transition
u	value of x for which turbulent spot leaves p
w	wall value (i.e., y = 0)
o	see x_o; see Eqn. 26
1, 2	y index (Eqn. 8); particular values (Eqns. 12 and 13)
δ^*	based on δ^*

Super Script

n	time level (see Table II)
• (dot)	time derivative
- (bar)	time average
' (prime)	fluctuating component
^ (carat)	amplitude (see Eqn. 11)